Bolometric light curves and explosion parameters of 38 stripped-envelope core-collapse supernovae

J. D. Lyman,[1,2]$\star$ D. Bersier,[2] P. A. James,[2] P. A. Mazzali,[2] J. J. Eldridge,[3] M. Fraser[4] and E. Pian[5,6]

[1]*Department of Physics, University of Warwick, Coventry CV4 7AL, UK*
[2]*Astrophysics Research Institute, Liverpool John Moores University, Liverpool L3 5RF, UK*
[3]*The Department of Physics, The University of Auckland, Private Bag 92019, Auckland, New Zealand*
[4]*Institute of Astronomy, University of Cambridge, Madingley Road, Cambridge CB3 0HA, UK*
[5]*INAF-Istituto di Astrofisica Spaziale e Fisica Cosmica, Via P. Gobetti 101, I-40129 Bologna, Italy*
[6]*Scuola Normale Superiore di Pisa, Piazza dei Cavalieri 7, I-56126 Pisa, Italy*

ABSTRACT

Literature data are collated for 38 stripped-envelope core-collapse supernovae (SE SNe; i.e. SNe IIb, Ib, Ic and Ic-BL) that have good light-curve coverage in more than one optical band. Using bolometric corrections derived in previous work, the bolometric light curve of each SN is recovered and template bolometric light curves provided. Peak light distributions and decay rates are investigated; SNe subtypes are not cleanly distinguished in this parameter space, although some grouping of types does occur and there is a suggestion of a Phillips-like relation for most SNe Ic-BL. The bolometric light curves are modelled with a simple analytical prescription and compared to results from more detailed modelling. Distributions of the explosion parameters show the extreme nature of SNe Ic-BL in terms of their ^{56}Ni mass and the kinetic energy, however ejected masses are similar to other subtypes. SNe Ib and Ic have very similar distributions of explosion parameters, indicating a similarity in progenitors. SNe IIb are the most homogeneous subtype and have the lowest average values for ^{56}Ni mass, ejected mass, and kinetic energy. Ejecta masses for each subtype and SE SNe as a whole are inconsistent with those expected from very massive stars. The majority of the ejecta mass distribution is well described by more moderately massive progenitors in binaries, indicating these are the dominant progenitor channel for SE SNe.

Key words: binaries: general – supernovae: general.

1 INTRODUCTION

Core-collapse supernovae (CCSNe) are the endpoints of massive stars. The observable signatures of these very luminous events exhibit strong heterogeneity, with several main subtypes existing amongst further, poorly known or peculiar events. The main classifications are made based on spectral information. Type II SNe (SNe II) exhibit strong, long-lasting hydrogen features in their spectra with Type Ib SNe (SNe Ib) being hydrogen deficient and type Ic SNe (SNe Ic) being hydrogen and helium deficient.[1] Intermediate to this broad Ibc/II division are Type IIb SNe (SNe IIb), with SN 1993J as the prototypical example of this class. SNe IIb initially show the strong hydrogen features that warrant an SN II classification, but subsequently evolve as an SN Ib after a period of

one to a few weeks (see Filippenko 1997, for a review of the spectral classification of SNe). A further designation of 'broad-line' (BL) is attached should the observed spectra reveal very large velocities for the ejecta (although there is no exact value for the dividing velocity, BL is generally assigned when a substantial fraction of the ejecta has velocities above that of ordinary SNe Ib/c, i.e. $\gtrsim$ 14 000 km s^{-1}). SNe Ic-BL have gathered much interest in recent years given their association with long-duration gamma-ray-bursts (GRBs; e.g. Galama et al. 1998; Stanek et al. 2003, see Hjorth & Bloom 2012 for a review). The lack of detected GRBs coincident with some SNe Ic-BL, such as SNe 2002ap (e.g. Gal-Yam, Ofek & Shemmer 2002), 2003jd (Valenti et al. 2008), 2009bb (Pignata et al. 2011) and 2010ah (Corsi et al. 2011; Mazzali et al. 2013), would suggest relativistic jet formation is not required to power BL SNe; although the case of associated off-axis GRBs is possible (Mazzali et al. 2005), for one event the geometry of the explosion makes this a less favourable scenario (Pignata et al. 2011). SNe IIb, Ib, Ic and Ic-BL are considered stripped-envelope SNe (SE SNe) since they display little to no hydrogen, indicating a massive hydrogen

---

$\star$E-mail: J.D.Lyman@warwick.ac.uk
[1] Although this does not exclude the presence of small amounts of hydrogen and/or helium in the pre-SN progenitors (Hachinger et al. 2012).

envelope is not present at the point of explosion, in contrast to SNe IIP.

The various observable signatures of CCSNe are linked to the state of the progenitor star upon explosion. The retention or not of a massive hydrogen envelope is dependent on the amount of mass-loss the progenitor experiences during its lifetime. Higher mass stars or stars in binary systems are expected to be able to shed their outer envelopes (and therefore explode as SE SNe), either via intrinsically high mass-loss rates for very high mass stars, or enhanced mass-loss due to a binary companion for more modest mass stars. Metallicity and rotation of the progenitor are also likely to increase the mass-loss, and hence the observed SN type. Observationally, SNe II are seen to be explosions from stars at the lower end of the massive star range ($\sim$8–16 $M_{\odot}$; see Smartt 2009, for a review),[2] which have not suffered sufficient mass-loss to remove their hydrogen envelopes. The introduction of binaries as the progenitors of at least a fraction of SE SNe, as backed up observationally (e.g. Maund et al. 2004; Ryder, Murrowood & Stathakis 2006; Smith et al. 2011; Folatelli et al. 2014b; Fox et al. 2014) and theoretically (e.g. Podsiadlowski, Joss & Hsu 1992; Podsiadlowski et al. 1993; Pols & Dewi 2002; Eldridge, Izzard & Tout 2008; Yoon, Woosley & Langer 2010; Claeys et al. 2011; Benvenuto, Bersten & Nomoto 2013; Bersten et al. 2014; Eldridge et al. 2013) would act to wash out any clear distinction between the masses of the progenitors, by allowing much more modestly massive stars to be stripped of their envelopes and making the binary parameters the dominant influence on the observed SN type. The current understanding of mass-loss from massive stars is encompassed in the review of Smith (2014), which includes a discussion of recent SN studies that favour the majority of SE SNe arising from binaries, with single, very massive Wolf–Rayet stars contributing a small fraction at most. This is consistent with studies showing most massive-stars are expected to have some form of interaction (mass transfer, merging etc.) with a companion during their evolution (e.g. Sana et al. 2012); this binary companion is also likely to be a massive star (Kobulnicky & Fryer 2007; Sana & Evans 2011), exacerbating the dearth of truly single very massive stars.

Direct detection studies in archival imaging can reveal the properties of the SN progenitor (e.g. Van Dyk, Li & Filippenko 2003; Smartt et al. 2004; Li et al. 2007; Gal-Yam & Leonard 2009; Van Dyk et al. 2012; Fraser et al. 2011, 2012; Maund et al. 2011; Van Dyk et al. 2013), but only for a very limited number of events. The requisite proximity of the SN and existence of pre-explosion deep, high-resolution imaging of the SN location restrict qualifying SN numbers severely and currently there is no confirmed progenitor detection of an SN Ib, Ic or Ic-BL (e.g. Maund & Smartt 2005; Crockett et al. 2007; Eldridge et al. 2013). However, the studies of Yoon et al. (2012) and Groh, Georgy & Ekström (2013a) show that even massive pre-SN stars are likely to be faint in optical bands, where direct detection studies occur, meaning present limits cannot be used to conclusively rule out very massive progenitors for SNe Ib/c. Although a high-mass star ($M_{ZAMS} \simeq 30$–40 $M_{\odot}$) was proposed as the progenitor of the SN Ib iPTF13bvn (Cao et al. 2013; Groh et al. 2013a) based on detections in pre-explosion imaging, the recent works of Fremling et al. (2014), Bersten et al. (2014) and Eldridge et al. (2015) argue against a single very massive progen-

itor, and favour a binary origin with a lower mass progenitor from both the pre-explosion imaging and studies of the SN light curve. Confirmation that the progenitor has faded in post-explosion imaging, possibly revealing the putative binary companion, is awaited at the time of writing to confirm the nature of the progenitor system.

Due to the severely restricted numbers of direct detection studies, other methods of SN investigation have provided new and complementary insights due to the much larger samples that can be obtained. Analysis of the hosts of SNe (e.g. Prieto, Stanek & Beacom 2008; Arcavi et al. 2010; Svensson et al. 2010; Kelly et al. 2014), the environments and metallicities of SN locations within the hosts (e.g. Anderson & James 2008; Boissier & Prantzos 2009; Anderson et al. 2010; Leloudas et al. 2011; Modjaz et al. 2011; Anderson et al. 2012; Kelly & Kirshner 2012; Crowther 2013), the stellar populations surrounding SNe (e.g. Kuncarayakti et al. 2013; Williams et al. 2014), and SN rates (e.g. Li et al. 2011; Smith et al. 2011) all provide alternate means of probing the underlying progenitors populations and investigating differences in age, metallicity, etc., between the subtypes. Results providing constraints on the ages/masses of SNe, generally to point to a mass sequence of increasing (*average*) initial mass for the SN subtypes of II → IIb → Ib → Ic → Ic-BL, albeit with significant overlap in the mass ranges. Rates of SE SNe compared to SNe II appear too high to only arise from the most massive stars, when considering the stellar initial mass function (IMF).

The luminous transient signature of an SN is also a rich source of information about the exploding star, as well as obviously informing on the manner of the explosion itself. Spectra are required in the first instance to type the SN, and, alongside spectral modelling codes (e.g. Mazzali & Lucy 1993; Jerkstrand, Fransson & Kozma 2011) and long-term monitoring, they can be used to infer the structure and stratification of the ejecta and reveal bulk parameters of the SN with good precision (e.g. Mazzali et al. 2007, 2013; Shivvers et al. 2013; Jerkstrand et al. 2015). As well as spectral information, the bolometric light curve of an SN is a useful tool for determining the nature of the explosion itself, and is used to correctly scale spectral analyses. Hydrodynamical modelling of SE SN bolometric light curves can be used to reveal the nature of the exploding stars giving constraints on the physical properties of the star upon explosion and the explosion parameters (e.g. Blinnikov et al. 1998; Tanaka et al. 2009; Bersten et al. 2014; Folatelli et al. 2014a; Fremling et al. 2014).

Unlike host galaxy/environmental analyses, study of the luminous transient signature from SNe is a time critical analysis. In order to properly infer the properties that led to the observed explosion, quick photometric and spectroscopic follow-up must occur (and continue for several months to tightly constrain models). Given the large SN discovery rates currently made possible by dedicated transient surveys (e.g. PTF and iPTF, Pan-STARRS, SkyMapper, La Silla-QUEST), such intense monitoring can only be afforded to select a few of the most interesting and observationally favourable events. This has meant a trade-off exists between studying individual objects with large data sets, or investigating a large number of SNe with poorer follow-up (e.g. Hamuy 2003; Drout et al. 2011). Cano (2013) addressed this issue by rescaling optical light curves of SNe Ib/c, Ic-BL and GRB-SNe based on their relative peak brightness and light-curve width to SN 1998bw, a very unusual SN. These rescaled light curves provided a means to model other SNe by scaling the explosion parameters found from modelling of SN 1998bw; the assumption being made that all SNe in the sample evolve spectrally and photometrically in a similar manner to SN 1998bw. It was found that SNe Ib and Ic are very similar in their explosion properties, with SNe Ic-BL and GRB-SNe exhibiting larger explosion

---

[2] The observed upper bound of this mass range may be uncertain due to mistreatment of reddening (Kochanek, Khan & Dai 2012; Walmswell & Eldridge 2012). This may reconcile observations with hydrodynamical modelling of SNe IIP, which generally infer higher masses (e.g. Utrobin & Chugai 2008, 2009; Bersten, Benvenuto & Hamuy 2011).

energies and higher ejected masses, pointing to a different progenitor channel for these SNe. They find results in broad agreement with previous studies, indicating scaling relations of SN 1998bw may be applied to other SE SNe, although the use of average photospheric velocities (see Section 2.2) for over half of the sample of SNe incurs large uncertainties in the results.

Here, we utilize a method that allows an SE SN to be modelled utilizing only two-filter optical follow-up and a peak-light spectrum. The bolometric corrections (BCs) to core-collapse SNe of Lyman, Bersier & James (2014, hereafter LBJ14) are used to provide a consistent, robust and accurate method of creating fully bolometric light curves for a large number of SE SNe from their optical colours. An analytical model (Arnett 1982; Valenti et al. 2008) is used to provide estimates of the bulk parameters of the explosions, fitted to each SN individually, which discern the nature of the progenitor system upon explosion.

Section 2 introduces the sample and describes the method of creating the bolometric light curves and the analytical method employed. Results are then presented and discussed in Sections 3 and 4, respectively.

2 METHOD

2.1 SN sample and data

BCs to CCSNe subtypes (SE and SNe IIP) are presented in LBJ14. The spectral energy distributions of a sample of literature SNe with ultraviolet, optical and near-infrared coverage (with corrections for flux outside the observed wavelength regime) were integrated and correlated with optical colours of the SN, to provide an accurate (rms <0.1 mag) method of determining the bolometric light curve of an SN with a polynomial fitted to optical colour. Since a method of creating bolometric light curves from just optical colours has been formulated, the creation of bolometric light curves is now not limited to those SNe with extended photometric coverage, but rather is possible for an SN with coverage in just two optical bands. Additional to this, distance and reddening determinations are needed in order to convert to luminosity and correct for the effects of dust.

The sample consists of literature SE SNe that have good light-curve coverage in at least two bands from which to construct a colour, which is in turn used to derive the BC. Here, the requirement of 'good' coverage refers to capturing at least the peak of the light curve (and preferably epochs on the rise) and at least several epochs within the next ∼60 d, extending at least 15 d past peak. Additionally, an optical spectrum near peak is required. We restrict our SNe to low redshift in order to avoid the need for *K*-corrections (see LBJ14). The sample consists of 9 IIb, 13 Ib, 8 Ic and 8 Ic-BL. The SN names, types, reddening values, distance moduli (to host) and colour(s) used for the BCs are presented in Table 1.

Photometric data were extracted from the literature for SNe in the sample (see references in Table 1). The same methods of light-curve dereddening and interpolation were employed as in LBJ14, in order to obtain values of simultaneous observations in the chosen filters, which give the colour. Extrapolations were not used for this analysis.

The reddening-corrected values of the chosen colour (see Table 1) were then fed into the BC polynomial fits of LBJ14 in order to recover the bolometric light curve. Some SNe were observed in a combination of Johnson–Cousins and Sloan optical filters – new BCs for these combinations were calculated following the method and data of LBJ14, the parameters for these new fits can be found in Table 2, with the corresponding fits for SNe II also presented for interest.

The resulting BC was then applied to the appropriate SN light curve (e.g. for colour *B − I*, the BC is applied to the *B*-band light curve). Using the distance modulus, we can convert m_{bol} to M_{bol} and finally to L_{bol}. For clarity in plotting, nearly contemporaneous data have been combined by averaging any epochs within 0.2 d of each other.

The results provide the largest sample of bolometric light curves for SE SNe thus far, on which a simple analytical model can be applied, in order to extract estimates for the explosion parameters.

2.2 The analytical model

The analytical model is based on that of Arnett (1982), and is appropriate for SE SNe, where the light curve is powered predominantly by the decay of ^{56}Ni (i.e. excluding interacting SNe). The model is fit over the photospheric phase, during the optically thick phase of the ejecta (up to ∼1–2 months after explosion, depending on the evolution-speed of the SN). The bolometric output is described by the model, and as such the model should be fitted to a bolometric light curve, with an additional constraint required in the form of a characteristic velocity of the ejecta (Section 2.2.1). From this simple analytical fitting, estimates of the mass of nickel synthesized (M_{Ni}) and the mass and kinetic energy of the ejecta (M_{ej} and E_K, respectively) can be made.

Naturally an analytical approximation requires some simplifying assumptions. These are listed in Arnett (1982) and Valenti et al. (2008), with brief discussion given here (see also discussion in Cano 2013).

(i) The radius is small at the onset of explosion. Although this is appropriate for most SE SNe progenitors, which have radii ∼R$_{\odot}$, up to ∼10 R$_{\odot}$ (but see Yoon et al. 2010), it may not be appropriate for some cases where an extended, low-mass envelope is present (e.g. SN 1993J, 2011hs), which can affect the light curve shortly after explosion. To minimize the impact of this very early signature on the overall light-curve model, very early data are not fit in our method.

(ii) Homologous expansion with spherical symmetry ($V \propto R$). SE SNe show evidence for some degree of asphericity of the ejecta, as gleaned from double-peaked nebular emission features (Maeda et al. 2008).

(iii) A constant opacity (κ_{opt}). In reality, this is dictated by the density and composition of the ejecta, and should therefore evolve with time. Here, κ_{opt} is set to be 0.06 cm^2 g^{-1} (e.g. Maeda et al. 2003; Valenti et al. 2011).

(iv) Centrally concentrated ^{56}Ni. The amount of mixing will affect the rise time of the SNe since radiation from high-velocity (i.e. further out in radius, given homologous expansion) ^{56}Ni will have a shorter diffusion time (Maeda et al. 2003; Dessart et al. 2012). 3D modelling has shown that a small fraction of high-velocity ^{56}Ni is not uncommon in SNe, although the bulk is generally located close to the centre (e.g. Hammer, Janka & Müller 2010).

(v) The decay of ^{56}Ni and ^{56}Co power the light curve. These radioactive isotopes represent the main source of energy of an SE SN, dominating the luminosity evolution for many months.

In the model, the photospheric-phase luminosity of an SN is described by equation A1 of Valenti et al. (2008), an update of the original Arnett (1982) model. The equation is fitted with two light-curve parameters, M_{Ni} and τ_m, which is given by

$$\tau_m^2 = \frac{2\kappa_{opt} M_{ej}}{\beta c v_{sc}}. \tag{1}$$

Table 1. Data for SNe used to create bolometric light curves References: (1) Richmond et al. (1994); (2) Matthews et al. (2002, and IAU circulars within); (3) Matheson et al. (2000); (4) Richmond et al. (1996); (5) Qiu et al. (1999); (6) Clocchiatti et al. (2011); (7) Benetti et al. (2011); (8) Stritzinger et al. (2002); (9) Mattila, Meikle & Chambers (2002); (10) Hasubick & Hornoch (2002); (11) Riffeser, Goessl & Ries (2002);(12) Motohara et al. (2002); (13) Gal-Yam et al. (2002); (14) Takada-Hidai, Aoki & Zhao (2002); (15) Yoshii et al. (2003); (16) Foley et al. (2003); (17) Hamuy et al. (2009); (18) Valenti et al. (2008); (19) Taubenberger et al. (2006); (20) Drout et al. (2011); (21) Tominaga et al. (2005); (22) Modjaz (2007); (23) Mirabal et al. (2006); (24) Bianco et al. (2014); (25) Stritzinger et al. (2009); (26) Hunter et al. (2009); (27) Sahu et al. (2009); (28) Roy et al. (2013); (29) Modjaz et al. (2009); (30) Taubenberger et al. (2011); (31) Pastorello et al. (2008); (32) Tsvetkov et al. (2009); (33) Pignata et al. (2011); (34) Valenti et al. (2011); (35) Olivares et al. (2012); (36) Valenti et al. (2012); (37) Ergon et al. (2014); (38) Bufano et al. (2014) (39) Fremling et al. (2014).

SN name	Type	$E(B-V)_{tot}$ (mag)	Distance modulus (mag)	Colour used	Refs.
1993J	IIb	0.194	27.81 ± 0.12	$B-I$	1–3
1994I	Ic	0.3	29.60 ± 0.10	$B-I$	4
1996cb	IIb	0.03	31.00 ± 0.31[a]	$B-R$	5
1998bw	Ic-BL	0.065	32.89 ± 0.15	$B-I$	6
1999dn	Ib	0.10	32.95 ± 0.11	$B-I$	7
1999ex	Ib	0.3	33.42 ± 0.25	$B-I$	8
2002ap	Ic-BL	0.09	29.50 ± 0.14	$B-I$	9–16
2003bg	IIb	0.02	31.68 ± 0.14	$B-I$	17
2003jd	Ic-BL	0.144	34.46 ± 0.20	$B-I$	18
2004aw	Ic	0.37	34.17 ± 0.19	$B-I$	19
2004dk	Ib	0.337	31.81 ± 0.18	$V-R$	20
2004dn	Ic	0.568	33.54 ± 0.16	$V-R$	20
2004fe	Ic	0.315	34.29 ± 0.15	$V-R$	20
2004ff	IIb[b]	0.302	34.82 ± 0.16	$V-R$	20
2004gq	Ib	0.253	32.07 ± 0.45	$V-R$	20
2005az	Ic[b]	0.441	32.96 ± 0.21	$V-R$	20
2005bf	Ib-pec	0.045	34.50 ± 0.27	$B-V$	21
2005hg	Ib	0.685	34.67 ± 0.15	$B-i$	22
2005kz	Ic-BL	0.514	35.30 ± 0.15	$V-R$	20
2005mf	Ic	0.398	35.27 ± 0.15	$B-i$	22
2006T	IIb	0.075[c]	32.58 ± 0.19	$B-i$	22
2006aj	Ic-BL	0.142	35.81 ± 0.10	$B-I$	23
2006el	IIb	0.303	34.23 ± 0.21	$V-R, V-i$[d]	20
2006ep	Ib	0.035[c]	33.84 ± 0.20	$B-i$	22,24
2007C	Ib	0.682	31.99 ± 0.25	$V-R$	20
2007Y	Ib	0.112	31.36 ± 0.14	$B-i$	25
2007gr	Ic	0.092	29.84 ± 0.16	$B-I$	26
2007ru	Ic-BL	0.27	34.15 ± 0.10	$B-I$	27
2007uy	Ib	0.63	32.40 ± 0.15	$B-V, B-I$[e]	28
2008D	Ib	0.6	32.46 ± 0.15	$B-I$	29
2008ax	IIb	0.4	29.92 ± 0.29	$B-I$	30,31,32
2009bb	Ic-BL	0.58	33.01 ± 0.15	$B-I$	33
2009jf	Ib	0.117	32.65 ± 0.10	$B-I$	34
2010bh	Ic-BL	0.507	36.90 ± 0.15	$g-i$	35
2011bm	Ic	0.064	34.90 ± 0.15	$B-I$	36
2011dh	IIb	0.07	29.46 ± 0.10	$B-I$	37
2011hs	IIb	0.17	31.85 ± 0.15	$B-I$	38
iPTF13bvn	Ib	0.07	31.76 ± 0.30	$B-I$	39

Notes. [a]Taken from NED.
[b]Updated SN classifications, presented in Modjaz et al. (2014), are used.
[c]Galactic extinction only.
[d]The $V-R$ correction was used for the rise to peak, with $V-i$ used for the peak and decline.
[e]The $B-V$ correction was used for early *Swift* data, with $B-I$ used for subsequent ground-based data.

Table 2. BCs for new filter combinations following method of LBJ14.

		SE SNe					SNe II			
x	y	$x-y$ range	c_0	c_1	c_2	rms	$x-y$ range	c_0	c_1	c_2	rms
B	i	−0.581 to 1.769	−0.186	−0.412	−0.172	0.061	−0.392 to 2.273	−0.155	−0.450	−0.167	0.023
V	i	−0.933 to 0.504	0.095	−0.320	−0.102	0.093	−0.391 to 0.658	0.181	−0.212	−1.137	0.044

$\beta \simeq 13.8$ is a constant, and c is the speed of light. v_{sc} is the *scale velocity* of the SN, which is observationally set as the photospheric velocity at maximum light (v_{ph}). As also noted by Wheeler, Johnson & Clocchiatti (2015), the initial relation for the scale velocity given by Arnett (1982, equation 54) is incorrect due to a typographical error – this error has been carried over into some subsequent studies using the model. With the simplifying assumptions of a constant density sphere undergoing homologous expansion, the relation should be

$$v_{sc}^2 \equiv v_{ph}^2 = \frac{5}{3}\frac{2E_K}{M_{ej}}. \tag{2}$$

The direct relation between τ_m, M_{ej} and E_K is therefore given by

$$\tau_m = \left(\frac{\kappa_{opt}}{\beta c}\right)^{0.5} \left(\Lambda \frac{M_{ej}^3}{E_k}\right)^{0.25}, \tag{3}$$

where $\Lambda = 6/5$. In Valenti et al. (2008), Λ is incorrectly given as 10/3, through propagation of the incorrect numerical factor (cf. their equation 2 and equation (2) – note that an exponent of two is also missing on v_{ph} in their equation). Although M_{ej}, determined from the photospheric phase, is related directly from the observed values of v_{ph} and τ_m, and thus not affected by this discrepancy, calculating E_K is. Where the typographical error is propagated in the literature, estimates of E_K from the model should be revised down by a factor $25/9 \, (= \frac{5}{3}/\frac{3}{5})$. However, this then results in a change (increase) in the ratio M_{ej}/E_K determined during the photospheric-phase. This further means that results from the two-zone *nebular phase* model (>60 d post-explosion; see Valenti et al. 2008, section 9 and appendix A and references therein for a description of this model) for SE SNe is affected. The nebular phase model accounts for a high-density inner component of the ejecta that is not emergent during the photospheric phase, *in addition* to the contribution of the ejecta component determined by the photospheric model. The time-scale of decay for the model is dictated by M_{ej}/E_K (Valenti et al. 2008, equations A10 and A11). The equations in the nebular model are separate from those of the photospheric model and thus their form is not explicitly affected by the typographical error. However, since a component of the nebular model is reliant on M_{ej}/E_K determined during the photospheric phase, the effects of the typographical error affect the fitting of the nebular phase model. We do not consider the nebular component here as we could not obtain satisfactory fits using the corrected formula. The primary issue was that the nebular phase model remained too bright (even when neglecting a further contribution from the inner, high-density component). This arises since an increase in M_{ej}/E_K means the time-scale for the evolution of the incomplete trapping of gamma rays becomes extended. For this reason, we take only values for M_{Ni}, M_{ej} and E_K derived from the photospheric-phase.

The photospheric phase of each light curve was fitted for M_{Ni} and τ_m (equation 1). τ_m was decomposed to M_{ej} and E_K using v_{ph} of the SN and equation (2). Photospheric data were only fit beginning $\lesssim 10$ d before peak, determined by early light-curve coverage. When fitting the model, data prior to 10 d before peak are not included in the fit since the assumptions in the model may not be appropriate. For example, an extended envelope can imprint on the rising light curve through cooling emission, post-shock-breakout. By restricting the time-range fitted, we become largely insensitive to the progenitor radius, and model only the ^{56}Ni and ^{56}Co powered emission, but we note that the contribution of any thin, extended envelope would not be included in our resulting parameters. The fitting of the analytical

functions to the light-curve data was done via the CURVE_FIT function in SCIPY.

2.2.1 Determining scale velocity of SNe

SNe exhibit strong P-Cygni line profiles in their spectra due to the fast moving ejecta. This causes absorption that is blueshifted by the velocity of the absorbing material relative to the rest wavelength of the spectral line. Due to the stratification of the ejecta and homologous expansion, elements towards the outer layers of the ejecta (e.g. helium and calcium) can exhibit large velocities compared to heavier, more centrally concentrated elements. Two elements chosen to better trace the photospheric velocity are silicon and iron, with Si II λ6355 and the Fe II set of lines clustered around 4500–5200 Å used.

Practically, the measurements of v_{ph} consist of a simple Gaussian fitting procedure to the absorption features of a wavelength- and flux-calibrated spectrum of the SN taken on or near peak, obtained from WISeREP (Yaron & Gal-Yam 2012)[3] and Modjaz et al. (2014), performed in the IRAF package SPLOT. This was performed for individual Fe II lines (Fe II λ4924, Fe II λ5018, Fe II λ5169), before averaging these values to obtain a value of v_{ph}. In the case where Fe II lines could not be accurately measured (e.g. strong line blending or no spectral coverage at those wavelengths), the Si II λ6355 feature was measured. When data were not available for an SN (i.e. we could not obtain a spectrum to analyse), we relied on values for v_{ph} that were found by other authors in the literature. These literature v_{ph} values were typically found using a similar Gaussian fitting technique or through spectral fitting. Measurements from this simple Gaussian-fitting method were found to agree well with those from detailed spectral fitting codes in the cases where a comparison was possible. Both methods have uncertainties of ~1000 km s^{-1}, which we take as a fiducial minimum uncertainty on our measurements (an additional uncertainty based on the epoch of the spectrum relative to peak is also added, see Section 3.3.1). This uncertainty arises from the data quality as well as the broad-featured characteristic of SNe spectra at maximum light – velocities of at least several thousands of km s^{-1}, as is seen for CCSNe, make line blending an issue and it is often the case that one cannot attribute a single absorption feature to one specific transition. Similarly, nearby emission from other transitions will also impact on the shape of the absorption feature, affecting the Gaussian fit and, ultimately, the photospheric velocity derived. Finally, in the absence of appropriate data or literature value for an SN, as was the case for SN 2005 kz, v_{ph} was taken to be the mean v_{ph} for the SN's type from the rest of the sample. Branch et al. (2002) provide a power-law fit to their estimates of the variation with time of v_{ph} values for SNe Ib (as determined from Fe II lines). The value at peak of this power law, ~9000 km s^{-1}, is in good agreement with the average SN Ib v_{ph} of 9900 km s^{-1} found here, given the uncertainties. The values of M_{ej} and E_K derived for SN 2005kz using this average v_{ph} are clearly susceptible to a larger systematic uncertainty, but the ^{56}Ni mass is unaffected.

3 RESULTS

3.1 Bolometric light curves

The bolometric light curves are presented in Fig. 1. The time and peak of each light curve (t_{peak} and M_{peak}, respectively) were found

---

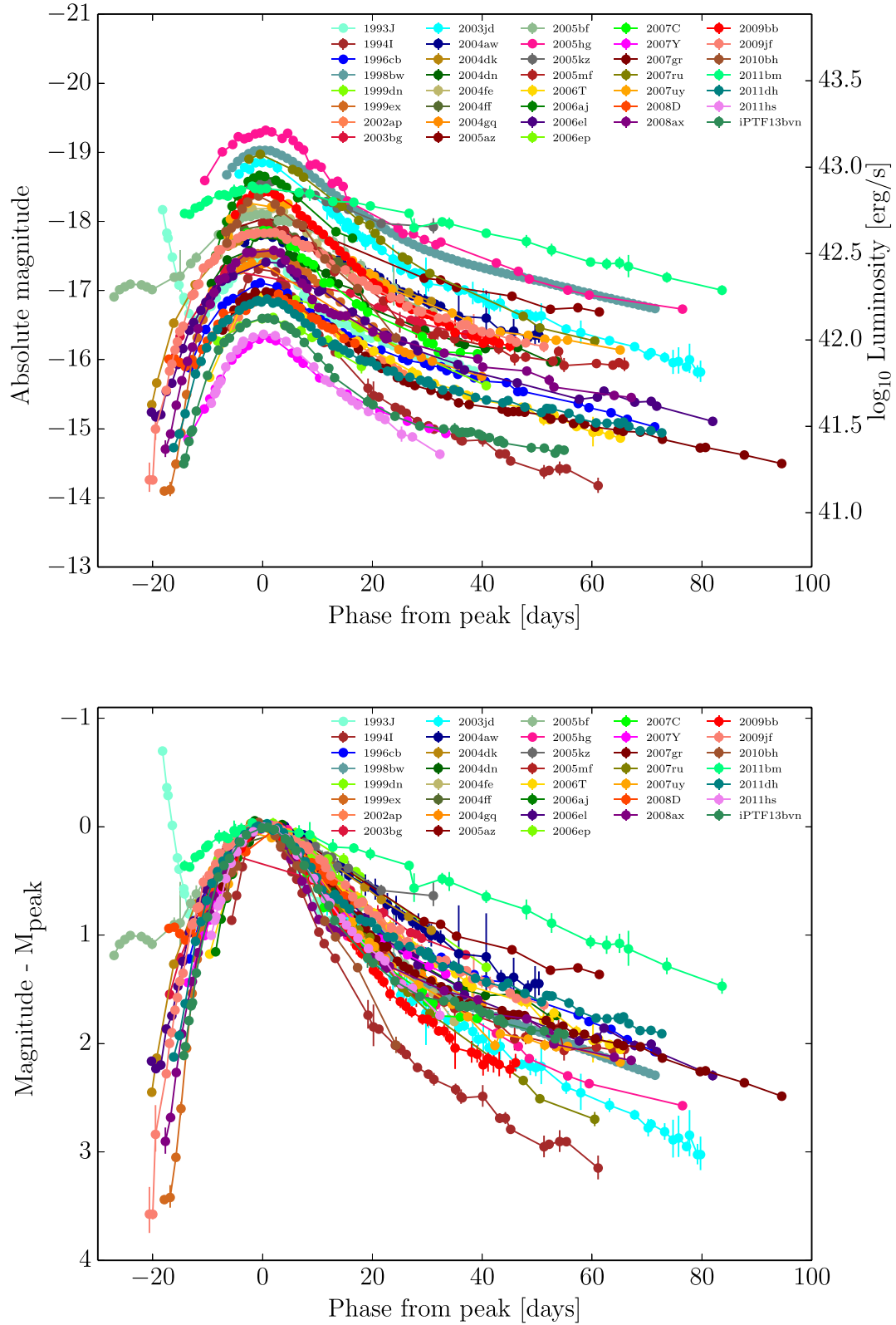[3] http://www.weizmann.ac.il/astrophysics/wiserep/

Figure 1. Bolometric light curves of SE SNe (top). The peak-normalized light curves are also displayed (bottom). Error bars are indicative of the uncertainty of the BC only, which is found by taking the uncertainty in the colour and translating that as an error on the BC fits. Distances, for example, will be a source of uncertainty in the top plot.

with a low-order polynomial, fitted to data around peak. The diversity of SE SNe becomes apparent from these plots. A roughly continuous spread over ∼3 mag is observed in M_{peak}; interestingly, two SNe Ib encompass the extremes of the spread, ranging from SN 2007Y[4] at $M_{peak} \sim -16.3$ to SN 2005hg at $M_{peak} \sim -19.2$.[5] This spread in M_{peak} is similar to that found by Drout et al. (2011) in their *V*- and *R*-band light curves when considering the overlapping sample. It should be noted that the photometry of SNe taken from Drout et al. (2011) may be systematically brighter than the intrinsic brightness of the SN since host-subtraction is not performed (Bianco et al. 2014), however we include only photometry from their 'gold' sample here, which appear more in agreement with host-subtracted photometry (Bianco et al. 2014), and remove very late-time data for SNe 2004dn and 2005mf, where flattening of the light curves was observed. As such, we consider this potential contamination to not significantly affect results or discussion.

The decline rates of the sample vary greatly; the speed of the evolution is parametrized by $\Delta m_{15,bol}$, which is the number of magnitudes from peak; the bolometric light curve has declined by 15 d after peak (values were found from polynomial fits to the light curves). SN 1994I, despite being often cited as a 'prototypical' SN Ic, has unusually fast evolution, as has been previously noted, with $\Delta m_{15,bol}$=1.37 calculated here. SN 2011bm displays the slowest evolution, with $\Delta m_{15,bol}$=0.20. The evolution speeds appear to form a continuum, as is evident from the bottom panel of Fig. 1, although SNe 1994I and 2011bm are noticeably displaced from the extremities of the distribution. Perhaps unexpectedly, a XRF-SN, SN 2010bh, is exceeded only by SN 1994I in terms of speed of evolution. This extremely fast evolution was noticed by Cano et al. (2011) and Olivares et al. (2012), but is highlighted here when compared to many other SE SNe. Such fast evolution is at odds with the perception of GRB/XRF-SN progenitors being very massive when considering the analytical form of SE SN light curves, since the time-scale of the evolution is directly related to M_{ej} (equation 1). The $\Delta m_{15,bol}$ values here are similar to the spread of preliminary values found for *V*, *r* and *i* bands by Bianco et al. (2014, see also Walker et al. 2014), whereas the values they find for bluer (redder) filters are systematically larger (smaller) than the average value for the bolometric light curves, indicative of the relative decline rates of these individual bands when compared to the bolometric light curve. No statistical distinction of the various subtypes can be made in $\Delta m_{15,bol}$, as was shown for the *V* and *R* band by Drout et al. (2011).

To investigate any possible correlation between light-curve peak and decline rate in SE SN bolometric light curves, $\Delta m_{15,bol}$ values are plotted against M_{peak} in Fig. 2. There appears to be a dearth of bright, slowly evolving and fast-and-faint SN, but the Spearman's rank coefficient (0.633) is not significant enough to reject the case of no correlation. There appears to be no reason why bright, slowly evolving SNe would be missed in surveys compared to quicker evolving events at similar luminosities, and it may indeed indicate that events such as SNe 2005kz and 2011bm are intrinsically rare.[6] Conversely, fainter, quickly evolving SNe (such as events similar to
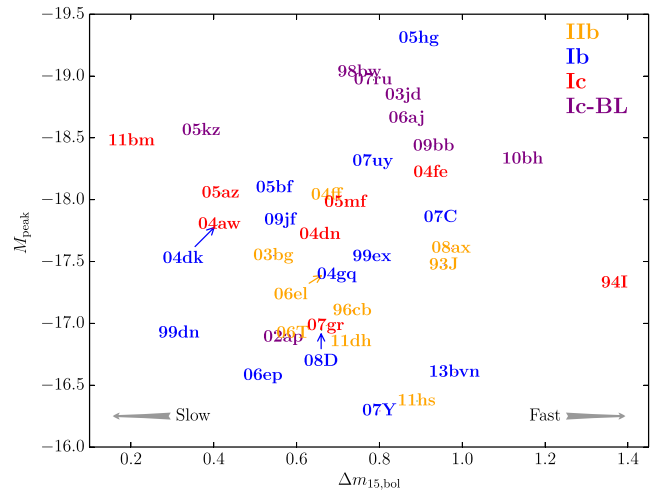

Figure 2. The peak magnitude of the evolution of the bolometric light curves against speed (parametrized as $\Delta m_{15,bol}$, see the text); the direction of light-curve evolution speed is denoted by the labelled grey arrows. The thin, coloured arrows indicate the true positions of SNe 2004dk, 2006el and 2008D, which have been offset for clarity. SNe are colour-coded according to their type.

SNe 2005ek; Drout et al. 2013, and 2010X; Kasliwal et al. 2010) are most likely to have been missed from detection (particularly prior to peak, which is one of the criteria imposed on this sample). As this is a literature-based sample, the selection effects cannot be analysed beyond these qualitative statements. The time and value of the light-curve peak and $\Delta m_{15,bol}$ value are listed for each SN in Table 3.

It is clear the various SN types do not inhabit exclusive regions of this parameter space, although some clustering of SNe IIb and SNe Ic-BL (with two exceptions) occurs. All SNe IIb in the sample occur within a small region of roughly average evolution speed and have modest-to-low peak magnitudes when compared to the entire sample. The decline rates of SNe IIb were noted to be distinct from the more slowly declining SNe IIP and IIL in the *R* band by Arcavi et al. (2012), and indeed found to be similar to those of SNe Ib and Ic. This is confirmed here for the bolometric light curve decline rates also. SNe Ic-BL are all luminous when compared to the rest of the sample with the exception of SN 2002ap, and all have fast evolution with the exceptions of SNe 2002ap and 2005 kz.

Template bolometric light curves for SE SNe are presented in Fig. 3, with dashed lines showing the median value and the coloured regions the standard deviation. The data for these templates are presented in Table A1 with the phases being relative to the peak of L_{bol}. These were found by sampling interpolations of the bolometric light curves and calculating the median and standard deviation of those SNe with a light curve covering that particular phase. (The median traces exhibit some mildly erratic behaviour due to the relatively small samples and the limited and non-uniform temporal coverage of the samples.) The templates reveal notable outliers in each case, emphasizing the heterogeneity of events even in these well-established SN types.

---

[4] The classification of SN 2007Y as an Ib has been questioned by Maurer et al. (2010) and Folatelli et al. (2014a), where detections of H α would favour a IIb classification.

[5] The classification of SN 2005hg was originally made as an SN Ic (Modjaz et al. 2005a), before the detection of He lines by Modjaz et al. (2005b).

[6] Another slowly evolving literature example is SN 1997ef – a very energetic SN Ic-BL (Mazzali, Iwamoto & Nomoto 2000), however this SN was not particularly bright, with $M_R \sim -17.2$ (Iwamoto et al. 2000). It is omitted in

this study since a bolometric light curve could not be constructed using the BC method presented.

Table 3. Bolometric light-curve properties for SE SNe.

SN	t_{peak} (MJD)	M_{peak} (mag)	$\Delta m_{15,bol}$ (mag)
1993J	49 094.4	−17.5	0.96
1994I	49 450.1	−17.3	1.37
1996cb	50 061.2	−17.1	0.73
1998bw	50 944.0	−19.0	0.75
1999dn	51 418.2	−16.9	0.32
1999ex	51 499.0	−17.5	0.78
2002ap	52 312.1	−16.9	0.57
2003bg	52 717.0	−17.5	0.54
2003jd	52 942.5	−18.8	0.86
2004aw	53 088.6	−17.8	0.41
2004dk	53 239.5	−17.8	0.41
2004dn	53 229.7	−17.7	0.66
2004fe	53 318.3	−18.2	0.92
2004ff	53 313.6	−18.0	0.67
2004gq	53 361.4	−17.4	0.70
2005az	53 473.9	−18.1	0.42
2005bf	53 497.8	−18.1	0.55
2005hg	53 681.7	−19.3	0.89
2005kz	53 710.5	−18.6	0.37
2005mf	53 733.4	−18.0	0.72
2006T	53 780.0	−16.9	0.59
2006aj	53 793.8	−18.7	0.87
2006el	53 983.6	−17.4	0.67
2006ep	53 988.5	−16.6	0.52
2007C	54 117.3	−17.9	0.95
2007Y	54 163.6	−16.3	0.80
2007gr	54 337.4	−17.0	0.67
2007ru	54 439.1	−19.0	0.78
2007uy	54 477.4	−18.3	0.78
2008D	54 492.5	−16.9	0.66
2008ax	54 548.8	−17.6	0.97
2009bb	54 920.9	−18.4	0.93
2009jf	55120.6	−17.8	0.56
2010bh	55 279.3	−18.3	1.15
2011bm	55 677.2	−18.5	0.20
2011dh	55 732.1	−16.9	0.73
2011hs	55 888.8	−16.4	0.89
iPTF13bvn	56 475.1	−16.6	0.98

3.2 Photospheric velocities

The v_{ph} values are presented in Table 4. These values were used to break the degeneracy in E_K and M_{ej} (Section 2.2). Velocity determinations were found to agree well with literature values that were determined from both the Gaussian-fitting technique and also spectral modelling. Where linear interpolations of v_{ph} were relied upon between epochs to obtain an estimate at peak, these were found to differ from using a Branch et al. (2002) power law by less than our assumed errors, reaching ∼700 km s^{-1} in the worst case for SN 2006T, but more typically ∼100–200 km s^{-1}. A correlation between the V-band magnitude and v_{ph} 50 d after explosion was found for SNe IIP by Hamuy (2003), whereas no correlation of v_{ph} with peak L_{bol} was found in the analysis of SE SNe here (this is discussed in Section 4.4 in the form of M_{Ni} against v_{ph}). Additionally, no correlation between v_{ph} and light curve decline rate ($\Delta m_{15,bol}$) was found here. Note that SN 2007uy was found to have a high v_{ph}, on the border of BL regime; however, the spectrum analysed was taken 3 d prior to peak and therefore has a more uncertain lower limit (as discussed later), and is thus considered an SN Ib in this study.
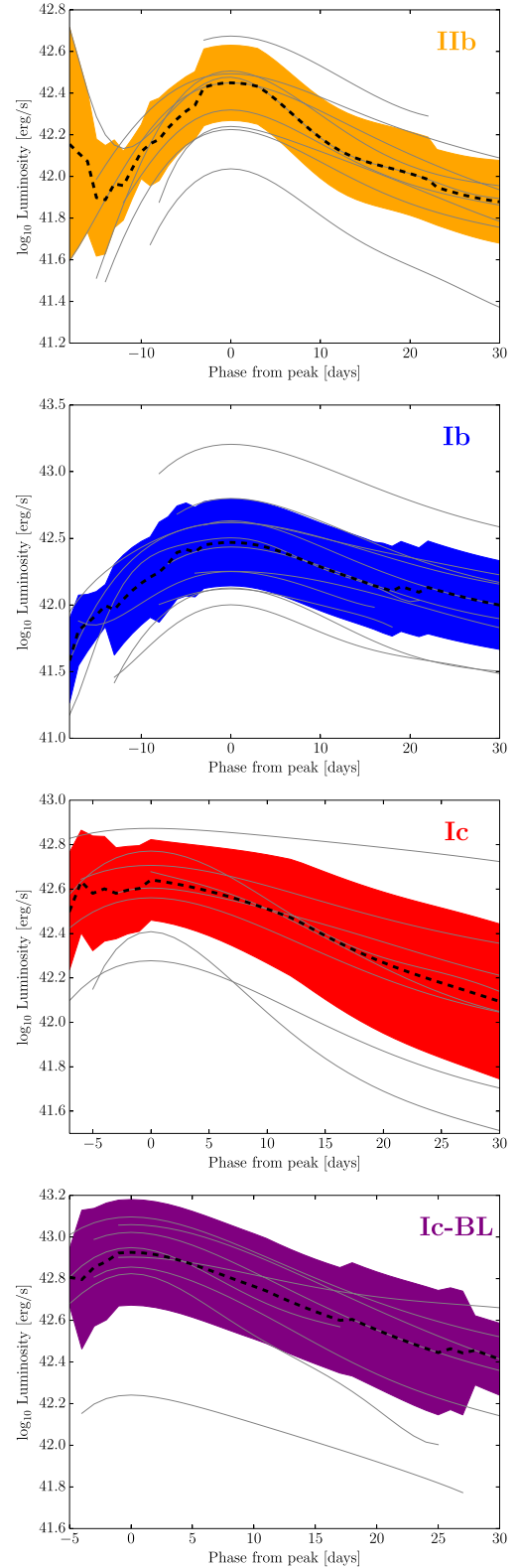

Figure 3. Template bolometric light curves for SE SNe, indicating the median value (black dashed line) and the standard deviation of the sample of light curves for that phase (coloured filled regions). Individual light curves are shown as thin solid lines.

Table 4. Photospheric velocity measurements for SE SNe.

SN name	Type	Line(s) used	v_{ph} (km s^{-1})	Phase[a] (d)	Notes
1993J	IIb	Fe II	8000 ± 1000	0	Agrees with Fe II velocities found by Ohta et al. (1994), Barbon et al. (1995) and Pastorello et al. (2008).
1994I	Ic	Fe II	$11\,500^{+1000}_{-1400}$	−1	Agrees with spectral modelling value of v_{ph} in Sauer et al. (2006) and Fe II velocity in Clocchiatti et al. (1996).
1996cb	IIb	Fe II	8500^{+1300}_{-1000}	1	Qiu et al. (1999), however, find a velocity of He I of 8870 km s^{-1} at epoch −15 d which would indicate extremely low v_{ph} at peak. Inconsistency was found when measuring velocities on the same spectrum, and the Fe II measurement found here is preferred.
1998bw	Ic-BL	Si II	$19\,500^{+1700}_{-1000}$	1	Fe II lines are largely blended. v_{ph} agrees with value found by Patat et al. (2001) and is similar to Si II velocity found by Pignata et al. (2011).
1999dn	Ib	Fe II	$10\,500 \pm 1000$	0	Taken from Benetti et al. (2011).
1999ex	Ib	Fe II	8500^{+1300}_{-1000}	1	Agrees with velocities given in Hamuy et al. (2002).
2002ap	Ic-BL	Fe II	$13\,000^{+2000}_{-1000}$	2	Gal-Yam et al. (2002) find the velocity of Si II to be 15 000 km s^{-1} at peak. Features blended somewhat.
2003bg	IIb	(Fe II)	8000 ± 1000	0	The value of v_{ph} from the spectral modelling of Mazzali et al. (2009) is used, this is consistent with an Fe II velocity found from a spectrum near peak.
2003jd	Ic-BL	Si II	$13\,500 \pm 1000$	0	Taken from Valenti et al. (2008).
2004aw	Ic	Fe II	$11\,000^{+1000}_{-1900}$	−2	Taubenberger et al. (2006) show a contemporaneous Si II velocity of 12 500 km s^{-1}.
2004dk	Ib	Si II	9200^{+1400}_{-1000}	1	Taken from Harutyunyan et al. (2008).
2004dn	Ic	Si II	$12\,500^{+1500}_{-1000}$	1	Taken from Harutyunyan et al. (2008).
2004fe	Ic	Fe II	$11\,000 \pm 1000$	0	–
2004ff	IIb	Fe II	$11\,000^{+1000}_{-2700}$	−4	–
2004gq	Ib	Fe II	$13\,000^{+1000}_{-1500}$	−1	Modjaz (2007) show a He I velocity of 14 000 km s^{-1} at peak.
2005az	Ic	Si II	9500^{+1400}_{-1000}	1	–
2005bf	Ib-pec	Fe II	7500^{+1800}_{-1000}	3	Matches value for Fe II lines found by Folatelli et al. (2006).
2005hg	Ib	Fe II	9000 ± 1000	0	Modjaz (2007) show a He I velocity of 10 000 km s^{-1} at peak.
2005kz	Ic-BL	n/a[b]	$19\,100 \pm 2500$	–	Filippenko, Foley & Matheson (2005) report a spectral similarity to SNe 1998bw and 2002ap.
2005mf	Ic	Fe II	$10\,000^{+1000}_{-1800}$	−2	–
2006T	IIb	Fe II	7500 ± 1000	0	Found from a linear interpolation of the Fe II velocities at −11 and +7 d from the spectra of Modjaz et al. (2014).
2006aj	Ic-BL	(Si II)	$18\,000 \pm 1000$	0	The value of v_{ph} presented in Pian et al. (2006) is used as the spectrum is noisy and heavily blended. This value agrees with that found by Pignata et al. (2011) from measuring Si II.
2006el	IIb	Fe II	$11\,000^{+1000}_{-2700}$	−4	A velocity of H β, somewhat past peak, is given as 11 500 km s^{-1} in Blondin et al. (2006).
2006ep	Ib	Fe II	9500 ± 1000	0	Found from a linear interpolation of the Fe II velocities at −8 and +8 d from the spectra of Modjaz et al. (2014).
2007C	Ib	Fe II	$11\,000^{+1000}_{-1400}$	−1	–
2007Y	Ib	Fe II	9000^{+1000}_{-1700}	−2	Matches the values for Fe II velocities found by Stritzinger et al. (2009) and Valenti et al. (2011).
2007gr	Ic	Fe II	$10\,000 \pm 1000$	0	Agrees with values from spectral modelling presented in Hunter et al. (2009).
2007ru	Ic-BL	Si II	$19\,000 \pm 1000$	0	Taken from Sahu et al. (2009).
2007uy	Ib	Fe II	$14\,000^{+1000}_{-2600}$	−3	Roy et al. (2013) find the velocity of He I to be 15 200 km s^{-1} at the same epoch.
2008D	Ib	Fe II	9500^{+2100}_{-1000}	3	Tanaka et al. (2009) determine a value of v_{ph} from spectral modelling in good agreement.
2008ax	IIb	Fe II	7500^{+2100}_{-1000}	4	Matches the values for Fe II velocities found by Pastorello et al. (2008) and Taubenberger et al. (2011).
2009bb	Ic-BL	Fe II	$17\,000^{+2900}_{-1000}$	3	Pignata et al. (2011) find Si II velocities at this epoch to be 18 000 km s^{-1} and find Fe II lines to be at 17 000 km s^{-1} using a spectral modelling code.
2009jf	Ib	Fe II	9500^{+2100}_{-1000}	3	Matches values found by Valenti et al. (2011).
2010bh	Ic-BL	Si II	$30\,000 \pm 1000$	0	Taken from Chornock et al. (2010) with linear interpolation between ∼−3 and ++13 d to get velocity at t_{peak}.
2011bm	Ic	Fe II	9000 ± 1000	0	Taken from Valenti et al. (2011).
2011dh	IIb	Fe II	7000 ± 1000	0	Taken from Bersten et al. (2012).
2011hs	IIb	Fe II	8000 ± 1000	0	Taken from Bufano et al. (2014) with linear interpolation ∼−2 and +7 d to get velocity at t_{peak}.
iPTF13bvn	Ib	Fe II	8000 ± 1000	0	Taken from Fremling et al. (2014) with linear interpolation ∼−2 and +1 d to get velocity at t_{peak}.

Notes. [a]Approximate phase measured relative to the bolometric light curve peak of spectrum used to measure v_{ph}.
[b]No value of v_{ph} could be measured or was available in the literature. The average v_{ph} for the SN type was used.

3.3 Explosion parameters

The results of the analytical modelling are given in Table 5, and some example fits are shown in Fig. 4.

As mentioned in Section 2.2, the propagation of a typographical error in the literature means some estimates of E_K, those that used the incorrect form, will be larger, with M_{ej} values also affected, depending on the specific model employed. Explosion parameter estimates here were found to broadly agree with those in the literature where an analytical model was applied to the SN (e.g. Taubenberger et al. 2006, 2011; Soderberg et al. 2008; Valenti et al. 2008, 2011;

Table 5. Results of explosion parameter modelling for SE SNe. (1) Utrobin (1994); (2) Woosley et al. (1994); (3) Young, Baron & Branch (1995); (4) Iwamoto et al. (1994); (5) Young et al. (1995); (6) Sauer et al. (2006)[b]; (7) Iwamoto et al. (1998); (8) Nakamura et al. (2001); (9) Stritzinger et al. (2002); (10) Mazzali et al. (2007)[b]; (11) Mazzali et al. (2009)[b]; (12) Maeda et al. (2007)[b]; (13) Mazzali et al. (2006a)[b]; (14) Stritzinger et al. (2009)[b]; (15) Mazzali et al. (2008)[b]; (16) Tanaka et al. (2009); (17) Hachinger et al. (2012)[b]; (18) Maurer et al. (2010)[b]; (19) Bersten et al. (2012); (20) Shivvers et al. (2013)[b]; (21) Bufano et al. (2014); (22) Fremling et al. (2014); (23) Bersten et al. (2014).

SN name	Type	τ_m (d)	$t_{peak}-t_0$ (d)	Phase fitted (d)	M_{Ni} ($M_\odot$)	M_{ej} ($M_\odot$)	E_K 10^{51} erg	M_{Ni} ($M_\odot$)	M_{ej} ($M_\odot$)	E_K (10^{51} erg)	Refs
					This study			**Literature values**			
1993J	IIb	14.7–15.5	18.3–19	−10, 10	$0.12^{+0.01}_{-0.01}$	$2.2^{+0.7}_{-0.5}$	$0.9^{+0.4}_{-0.3}$	0.06–0.14	1.9–3.5	1–1.6	(1–3)
1994I	Ic	5.6–7.3	8.6–10	−5, 10	$0.07^{+0.01}_{-0.01}$	$0.6^{+0.3}_{-0.1}$	$0.4^{+0.2}_{-0.2}$	0.07	0.9–1.3	1	(4–6)
1996cb	IIb	12.0–15.3	15.5–18.5	−10, 10	$0.09^{+0.03}_{-0.02}$	$1.7^{+1.0}_{-0.4}$	$0.7^{+0.6}_{-0.3}$	–	–	–	–
1998bw	Ic-BL	13.2–13.2	15.1	−8, 10	$0.54^{+0.08}_{-0.07}$	$4.4^{+1.2}_{-0.8}$	$9.9^{+3.8}_{-2.2}$	0.4–0.7	∼10	20–50	(7,8)
1999dn	Ib	13.9–17.4	14–18.5	−4, 15	$0.10^{+0.01}_{-0.02}$	$4.0^{+1.1}_{-1.7}$	$2.7^{+1.1}_{-1.3}$	–	–	–	–
1999ex	Ib	15.5–16.9	18–19	−10, 15	$0.15^{+0.04}_{-0.03}$	$2.9^{+0.9}_{-0.7}$	$1.3^{+0.8}_{-0.5}$	∼0.16	–	∼2.7	(9)
2002ap	Ic-BL	9.1–12.2	11–13.9	−6, 15	$0.07^{+0.01}_{-0.01}$	$2.0^{+0.8}_{-0.7}$	$2.0^{+1.3}_{-0.9}$	0.11	2.5	4	(10)
2003bg	IIb	17.7–19.7	22–23	−15, 21	$0.15^{+0.02}_{-0.02}$	$3.5^{+1.1}_{-0.8}$	$1.4^{+0.7}_{-0.5}$	0.15–0.20	4–5	5	(11)
2003jd	Ic-BL	11.9–13.2	14.3–15.3	−6, 10	$0.43^{+0.09}_{-0.07}$	$2.5^{+0.9}_{-0.5}$	$2.7^{+1.1}_{-0.7}$	–	–	–	–
2004aw	Ic	14.6–15.8	15.8–17	−5, 8	$0.20^{+0.04}_{-0.03}$	$3.3^{+0.9}_{-0.8}$	$2.4^{+0.9}_{-1.1}$	–	–	–	–
2004dk	Ib	15.9–19.0	18.2–21	−7, 12	$0.22^{+0.04}_{-0.04}$	$3.7^{+1.3}_{-1.0}$	$1.8^{+1.1}_{-0.7}$	–	–	–	–
2004dn	Ic	10.2–14.4	14.3–17.3	−9, 13	$0.16^{+0.03}_{-0.03}$	$2.8^{+1.0}_{-1.2}$	$2.6^{+1.3}_{-1.2}$	–	–	–	–
2004fe	Ic	9.3–12.5	12.5–14.9	−7, 10	$0.23^{+0.04}_{-0.04}$	$1.8^{+0.7}_{-0.7}$	$1.3^{+0.6}_{-0.6}$	–	–	–	–
2004ff	IIb	9.0–12.1	11–15	−4, 15	$0.18^{+0.03}_{-0.03}$	$1.5^{+0.7}_{-0.5}$	$1.1^{+0.6}_{-0.7}$	–	–	–	–
2004gq	Ib	9.5–12.7	13–15.5	−5, 1	$0.10^{+0.05}_{-0.04}$	$1.8^{+1.0}_{-0.5}$	$1.9^{+1.1}_{-0.7}$	–	–	–	–
2005az	Ic	13.0–16.9	16–20	−7, 30	$0.24^{+0.05}_{-0.04}$	$2.6^{+1.2}_{-0.8}$	$1.4^{+0.9}_{-0.6}$	–	–	–	–
2005bf	Ib	9.2–14.5	13–17	−8, 6	$0.07^{+0.03}_{-0.02}$	$0.8^{+1.2}_{-0.2}$	$0.3^{+0.5}_{-0.1}$	0.08	–	–	(12)
2005hg	Ib	11.0–13.4	15–18	−8, 15	$0.66^{+0.10}_{-0.09}$	$1.9^{+0.6}_{-0.6}$	$0.9^{+0.4}_{-0.4}$	–	–	–	–
2005kz	Ic-BL	15.8–21.1	17–25	−3, 15	$0.45^{+0.09}_{-0.07}$	$8.1^{+3.7}_{-2.6}$	$17.6^{+11.1}_{-7.9}$	–	–	–	–
2005mf	Ic	9.8–13.5	12–20	−1, 14	$0.17^{+0.06}_{-0.02}$	$1.4^{+1.0}_{-0.4}$	$0.9^{+0.7}_{-0.4}$	–	–	–	–
2006T[a]	IIb	10.9–12.6	16–18	−5, 15	$0.07^{+0.03}_{-0.01}$	$1.3^{+0.5}_{-0.3}$	$0.4^{+0.2}_{-0.2}$	–	–	–	–
2006aj	Ic-BL	7.7	9.6	−5, 15	$0.28^{+0.03}_{-0.02}$	$1.4^{+0.4}_{-0.2}$	$2.7^{+0.8}_{-0.6}$	0.21	2	2	(13)
2006el	IIb	14.2–16.6	17.8–19.5	−10, 12	$0.13^{+0.03}_{-0.02}$	$3.3^{+1.1}_{-1.0}$	$2.4^{+1.0}_{-1.5}$	–	–	–	–
2006ep[a]	Ib	10.8–17.3	15–20	−8, 14	$0.06^{+0.03}_{-0.01}$	$2.7^{+1.3}_{-1.3}$	$1.4^{+0.8}_{-0.8}$	–	–	–	–
2007C	Ib	8.7–12.9	12.5–17	−7, 10	$0.17^{+0.04}_{-0.04}$	$1.9^{+0.7}_{-0.9}$	$1.4^{+0.6}_{-0.8}$	–	–	–	–
2007Y	Ib	10.9–14.9	13.6–17	−7, 11	$0.04^{+0.01}_{-0.00}$	$1.4^{+1.3}_{-0.4}$	$0.7^{+0.7}_{-0.3}$	0.06	–	–	(14)
2007gr	Ic	10.9–12.9	13.5–15	−5, 9	$0.08^{+0.01}_{-0.01}$	$1.8^{+0.6}_{-0.4}$	$1.1^{+0.5}_{-0.4}$	–	–	–	–
2007ru	Ic-BL	6.8–11.2	9–14	−3, 14	$0.41^{+0.05}_{-0.06}$	$2.2^{+1.1}_{-1.1}$	$4.7^{+2.4}_{-2.5}$	–	–	–	–
2007uy	Ib	12.5–14.7	15–16.5	−6, 6	$0.28^{+0.04}_{-0.04}$	$3.3^{+1.1}_{-1.0}$	$3.9^{+1.5}_{-2.0}$	–	–	–	–
2008D	Ib	15.4	17.9	−10, 12	$0.09^{+0.01}_{-0.01}$	$2.9^{+1.0}_{-0.6}$	$1.6^{+1.3}_{-0.5}$	0.07–0.1	4.3–7	3.5–8.5	(15,16)
2008ax	IIb	16.7–17.0	19.3–19.6	−8, 13	$0.15^{+0.05}_{-0.03}$	$2.8^{+1.0}_{-0.6}$	$0.9^{+1.1}_{-0.4}$	0.09–0.12	2.2–3.2	0.7–1.7	(17,18)
2009bb	Ic-BL	8.5–10.0	11.2–12.4	−5, 10	$0.25^{+0.04}_{-0.03}$	$1.9^{+0.6}_{-0.5}$	$3.3^{+2.2}_{-1.0}$	–	–	–	–
2009jf	Ib	18.4–21.8	20.5–22.5	−10, 15	$0.24^{+0.03}_{-0.02}$	$4.7^{+1.7}_{-1.1}$	$2.5^{+2.2}_{-0.9}$	–	–	–	–
2010bh	Ic-BL	4.9	8.2	−5, 10	$0.17^{+0.03}_{-0.02}$	$0.9^{+0.2}_{-0.2}$	$4.9^{+1.3}_{-1.0}$	–	–	–	–
2011bm	Ic	28.3–30.4	30.3–32.3	−10, 13	$0.62^{+0.09}_{-0.08}$	$10.1^{+2.8}_{-2.3}$	$4.9^{+2.2}_{-1.7}$	–	–	–	–
2011dh	IIb	15.5–16.0	19.2–19.8	−8, 13	$0.08^{+0.02}_{-0.02}$	$2.2^{+0.6}_{-0.5}$	$0.7^{+0.4}_{-0.3}$	0.07–0.08	1.8–2.5	0.6–1	(19,20)
2011hs	IIb	8.8–12.1	11.4–14.4	−5, 10	$0.04^{+0.01}_{-0.01}$	$1.0^{+0.8}_{-0.3}$	$0.4^{+0.3}_{-0.2}$	0.04	1.8–2.5	0.8–0.9	(21)
iPTF13bvn	Ib	12.5–13.4	15.6–16.2	−9, 10	$0.06^{+0.02}_{-0.01}$	$1.7^{+0.5}_{-0.4}$	$0.7^{+0.3}_{-0.2}$	0.05–0.10	1.9–2.3	0.7–0.9	(22,23)

Notes. [a]Only Galactic extinction is accounted for, thus the M_{Ni} value has a large upper uncertainty arising from the possibility of significant, unaccounted for, reddening.

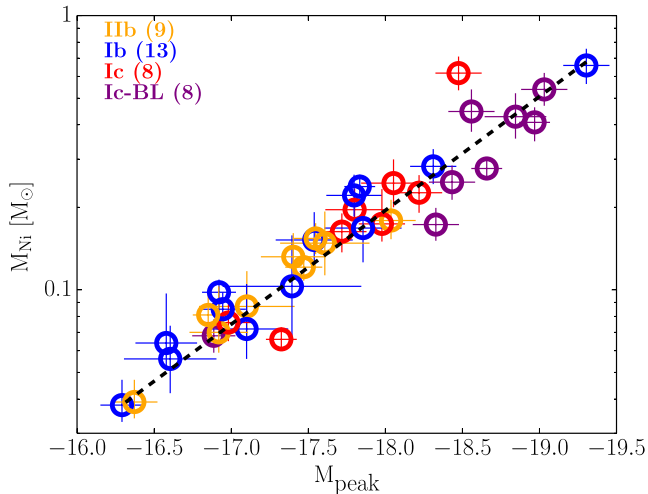[b]Spectral modelling of SNe, other references relate to hydrodynamical modelling.

Figure 4. Some examples of the fits found when modelling the bolometric light curves with the analytical prescription (examples of SNe IIb, Ib, Ic and Ic-BL from top to bottom). Data points in blue indicate those that were used in the fitting routine.

Benetti et al. 2011; Drout et al. 2011; Pignata et al. 2011; Cano 2013; Roy et al. 2013; Taddia et al. 2015) modulo the differences arising from choices of numerical factors. Differing values of Λ in equation (3) are used, for example Cano (2013) have $\Lambda = 1$ as they use $v_{ph}^2 = 2E_K/M_{ej}$, whereas we use $\Lambda = 6/5$ given our form of v_{ph} (equation 2). This numerical factor difference is likely partly responsible for the somewhat smaller (albeit consistent) E_K values for the subtype averages we find compared to Cano (2013), as discussed later. Differing numerical factor choices will affect the absolute parameter values but not the relative differences (e.g. between subtype averages). Previous literature modelling was done either through a direct fitting of the model, as is done here, or using scaling relations for the peak and width of the light curve and appropriately scaling the values of a better-studied SN by assuming similarity in the other properties of the explosion. Although agreement between the results is reassuring, we stress that estimates from such modelling are subject to sizeable uncertainties and differences in estimates are largely driven by the respective choices of v_{ph}, κ_{opt} etc., making a detailed consistency analysis of limited value.

For the events where such studies have been performed, we present in Table 5 values for the SN explosion parameters determined by more detailed spectral or hydrodynamical modelling in order to make comparisons. Generally, adopted values of distance and reddening match those in the literature works, when they are specified, however see Section 3.3.2 for a discussion directly comparing results from the two methods. On the whole, given the simplifications inherent in the analytical model, the estimates are in reasonable agreement for the majority of events and thus the analytical prescription provides an inexpensive method to obtain population statistics for SNe, however there are some notable departures between the two methods. For example, the M_{ej} and E_K for SNe 1998bw and 2008D are lower than estimates from hydrodynamical modelling. Section 3.3.2 contains direct comparison between results from the model employed here and those of more detailed modelling, with further discussion of the discrepancies. The average values for each SN type are shown in Table 6. SN 2005bf was a very unusual event that displayed a double-humped light curve. There have been various models proposed for the SN with different energy sources powering the second, brighter hump.

Among these, ^{56}Ni decay has been proposed, and, given the high peak luminosity, $\sim 5 \times 10^{42}$ erg s^{-1}, this requires $M_{Ni} \sim 0.32$ M$_\odot$ to power it (Tominaga et al. 2005). However, Maeda et al. (2007), from nebular spectral modelling, find that $\lesssim 0.08$ M$_\odot$ of ^{56}Ni was synthesized, inconsistent with an ^{56}Ni-powered explanation for the second peak. Here, the analytical model was used over the first 'pre-cursor' hump, which reveals an ^{56}Ni mass ($M_{Ni} \sim 0.07$ M$_\odot$) that is in good agreement to the value derived from nebular spectral modelling, suggesting that the second hump indeed has some other power source (e.g. magnetar, Maeda et al. 2007). We note that the particularly unusual nature of this SN may compromise the M_{ej} and E_K determinations from such simple modelling.

A fit to M_{peak} and M_{Ni} values found from this modelling is presented in Fig. 5, with the best-fitting relation given by

$$\log_{10} M_{Ni} = -0.415 \times M_{peak} - 8.184. \tag{4}$$

The rms of M_{Ni} values around the fit is 0.064 M$_\odot$. This is analogous to the relations presented in Perets et al. (2010) and Drout et al. (2011), here in terms of the bolometric luminosity.

3.3.1 Uncertainties in derived parameters

In this section, we describe the contributing factors to the uncertainties given in Table 5.[7]

The value primarily affecting M_{Ni} is the peak of the light curve and it is thus dependent on the distance determination. Literature uncertainties for μ to each SN host were used (see references in Table 1), or, where no literature value existed, the spread in the distance modulus determinations for the host, as given in the NASA/IPAC Extragalactic Database (NED), was used. Typical uncertainties were 0.1–0.2 mag, i.e. an uncertainty of $\sim$10–20 per cent in luminosity and thus corresponding uncertainty in M_{Ni}. Uncertainties on $E(B - V)$ affect the BC used, however the change in the BC is small for SE SNe colours at peak (see further discussion in LBJ14). Since many reddening values did not have an accompanying uncertainty, we simply use the estimate for each event that is given in the literature. The determinations of M_{Ni} for SNe 2006T and 2006ep have more uncertain upper limits, found by assuming that they suffer the median $E(B - V)_{host}$ of the sample. Reddening and distance uncertainties mainly represent a scaling uncertainty on the light curve (e.g. Ergon et al. 2014) and thus affect M_{ej} and E_K little.

M_{ej} and E_K are susceptible to uncertainties arising from a number of sources. One such source is the uncertainty on v_{ph}. The errors on v_{ph} were found by taking into account both intrinsic uncertainties in the fitting method ($\sim$1000 km s^{-1}) as well as accounting for the fact that not all spectra were directly observed at peak. For example, a v_{ph} determination before peak could overestimate v_{ph} at peak and similarly underestimate it for a determination after peak. Therefore v_{ph} values derived from spectra before (after) peak had an additional component to the lower (upper) error budget. The power law of Branch et al. (2002, $v_{ph} \propto t^{-2/(n-1)}$, where $n = 3.6$) was used as a gauge of the size of this potential offset from the v_{ph} at peak, with a fiducial peak time of 20 d. Fe II lines were assumed to trace v_{ph}, although in some cases Si II had to be used due to strong blending of Fe II lines, which may be systematically offset due to contamination from other species. The error on the v_{ph} value of SN 2005kz, which was assigned the average v_{ph} for its type is taken to be 2500 km s^{-1}.

---

[7] Statistical uncertainties quoted by the fitting procedure were found to be much less than the errors detailed and as such are not included.

Table 6. Average v_{ph} and explosion parameters for SE SN types.

SN type	v_{ph} (km s^{-1})		M_{Ni} (M$_\odot$)		M_{ej} (M$_\odot$)		E_K (10^{51} erg)	
	Mean	Sth. dev.	Mean	Std. dev.	Mean	Sth. dev.	Mean	Sth. dev.
IIb	8300	750	0.11	0.04	2.2	0.8	1.0	0.6
Ib	9900	1400	0.17	0.16	2.6	1.1	1.6	0.9
Ic	10 400	1200	0.22	0.16	3.0	2.8	1.9	1.3
Ic-BL	19 100	5000	0.32	0.15	2.9	2.2	6.0	5.0

Additionally, the choice of κ_{opt} directly affects M_{ej} and E_K for a given τ_m (equation 1), in that it acts to scale these values. The choice of constant opacity is a limitation of this simple modelling scheme, whereas, as mentioned previously, this will evolve with time based on the composition and temperature of the ejecta. We take a 20 per cent uncertainty in our choice of $\kappa_{opt} = 0.06$ cm^2 g^{-1}; previous studies have assumed values of 0.05 (Drout et al. 2011), 0.06 (Maeda et al. 2003; Valenti et al. 2008), 0.07 (Cano 2013; Taddia et al. 2015) and 0.08 cm^2 g^{-1} (Pignata et al. 2011), largely driven by the values of κ_{opt} near peak from results of spectroscopic modelling (Chugai 2000; Mazzali et al. 2000, 2013; Mazzali et al., in preparation). These line-based opacities (i.e. neglecting continuum opacity; see Mazzali et al. 2001) include time-dependant evolution due to, e.g. the temperature of the ejecta. Furthermore, different composition of the ejecta, in particular when considering different SE SN subtypes, will affect the opacity, although variations in ejecta abundances (e.g. CO/He) amongst SNe is not well known at present. As such, a single choice of opacity represent a simplifying assumption of the model, which deserves further investigation to assess its impact on results for different SE SNe subtypes across the parameter space of SN explosions. With other values fixed, this uncertainty contributes an uncertainty of $+25/-17$ per cent in M_{ej} and E_K determinations (since both have the same dependence on κ_{opt}[8]). An in-depth study of the evolution of the opacity for SE SNe is beyond the scope of this paper, but the results of such a study would be useful to constrain the applicability of such analytical models where a constant value of κ_{opt} is used.

Finally, the analytical model requires an initial starting time, t_0, which affects the value of τ_m that is fitted and also M_{Ni}. Where appropriate (e.g. in the case of GRB-SNe), this additional uncertainty did not factor since t_0 is known. Where t_0 was very poorly constrained, the model was manually fitted for a variety of τ_m values where the model still reasonably reproduced the observed light curve. The range of t_0 used for each SN is shown in Table 5. We note in passing, in agreement with the concurrent work of Taddia et al. (2015, but here regarding the bolometric rise), we find, for our subtype averages, SNe Ic-BL exhibit the shortest rise times to peak, with SNe Ib and IIb having similar rise times. We also find the average SNe Ic to be similar to the rise times to SNe Ib and IIb, but this is complicated by SN 2011bm, which Taddia et al. (2015) exclude from their sample. The distribution of rise times are plotted in Fig. 6, however the interested reader is directed to Taddia et al. (2015) for a more thorough discussion of rise times. The error on M_{Ni} arising from varying t_0 was $\lesssim 0.01$ M$_\odot$ where it was varied over ~ 1–2 d. For the least constrained events, the M_{Ni} uncertainty was 10–15 per cent. M_{ej} and E_K errors were 10–30 per cent for reasonably well constrained events (1–2 d) but $+(30$ to $40)/-(15$ to $25)$ per cent for the more unconstrained events (e.g. SN 2011 hs).

Total uncertainties on the parameters were found by refitting the model for all varying parameters and adding in quadrature the uncertainty from each parameter, these are given in Table 5.

We note that the asphericity of the explosions, which breaks the assumption of spherical symmetry in the model (Section 2.2), contributes a systematic uncertainty in our results. It appears some degree of asphericity is near-ubiquitous in SE SNe around peak light (see the review of Wang & Wheeler 2008). One may expect the very energetic SNe Ic-BL (and GRB-SNe) to display the strongest asymmetries, although their global asymmetries appear to be $\lesssim 15$ per cent (e.g. Wang et al. 2003; Maund et al. 2007a, for SNe 2002ap and 2006aj, respectively) and indeed a normal SN Ic, SN 1997X showed one of the strongest degrees of polarization, indicating a high degree of asymmetry (Wang et al. 2001). The uncertainty due to asphericity is higher in the more stripped SNe Ic and Ic BL, where stronger asymmetries in the deep ejecta (Wang & Wheeler 2008) can influence the photosphere during evolution around peak light. It is likely to be less pronounced in SNe IIb around peak owing to the presence of the hydrogen envelope (Maund et al. 2007b). Our results, based on a spherically symmetric model, could be described as the isotropic-equivalent values for the SNe (Wang et al. 2003).

3.3.2 Direct comparison to detailed modelling

Here, a recent subset of SNe with explosion parameters derived from hydrodynamical modelling of the light curve, to which we can compare our results, is presented. In order to make a comparison, external factors common to both methods such as distance, reddening and the time of explosion were set to those of the comparison works. Due to the inherent differences in the models, such as the lack of treatment for evolution of κ_{opt} or v_{ph} in the analytical model, just the best-fitted parameters are given for direct comparison (i.e. neglecting our uncertainties in these values).

A note must also be made regarding the new bolometric light curve creation method of LBJ14, used here. Although this has been used for some recent events, other methods of forming bolometric light curves have been used by other studies. For example, discrepancies between our derived M_{Ni} to that of, e.g. Utrobin (1994), where the bolometric light curve was created from *BVRI* photometry alone, is dominated by the light curve creation method – only ~ 50–60 per cent of the bolometric flux from an SE SN is emitted in these bands (LBJ14). As such, we restrict comparisons to those where a good approximation of the bolometric light curve is used – where appropriate, the method used to create this is highlighted in the discussion. We also note that many of the SNe in the current sample also formed part of the original SN sample of LBJ14, as such we can be confident our method is not introducing some large systematic uncertainty in the resulting bolometric light curves.

3.3.2.1 SN 2008D. We use the same distance and t_0 (time of the X-ray flash) as those of Tanaka et al. (2009). Our $E(B - V) = 0.6$ mag is also consistent with the value used by these studies of 0.65 mag at a level where derived parameters will not be affected

---

[8] Using equations (1) and (2): $M_{ej}^3/E_K \propto \kappa_{opt}^{-2} \rightarrow M_{ej} \propto \kappa_{opt}^{-1} v_{ph}$, given $E_K/M_{ej} \propto v_{ph}^2$ – and therefore $E_K \propto \kappa_{opt}^{-1} v_{ph}^3$.
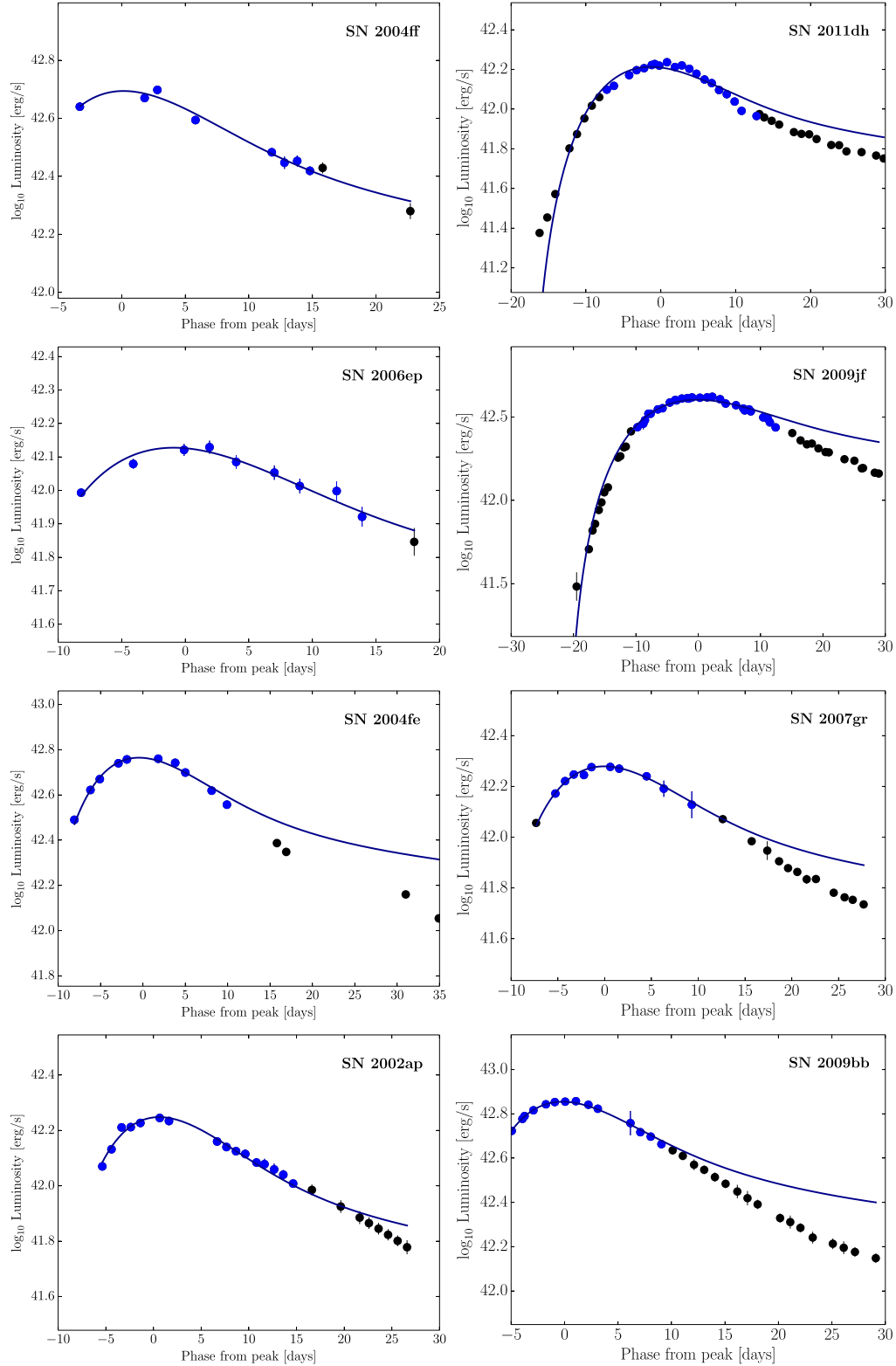
Figure 5. Relationship between bolometric peak, M_{peak}, and the M_{Ni} value derived from analytical modelling for SE SNe. Note the 'peak' of SN 2005bf is taken as the pre-cursor at $M_{peak} \sim -17.1$, see the text. The best-fitting loglinear relation is shown (equation 4). SNe are colour coded by type.

beyond the precision quoted. Tanaka et al. (2009) obtain parameters of $M_{Ni} \sim 0.07$ $M_\odot$, $M_{ej} = 5.3 \pm 1.0$ $M_\odot$ and $E_K = 6.0 \pm 2.5 \times 10^{51}$ erg through hydrodynamical modelling. Our results give $M_{Ni} = 0.09$ $M_\odot$, $M_{ej} = 2.9$ $M_\odot$ and $E_K = 1.6 \times 10^{51}$ erg. M_{ej} and E_K

estimate here are much lower than those from hydrodynamical modelling. Similarly lower estimates were also made using analytical relations by Soderberg et al. (2008). The cause of this disagreement is discussed in Tanaka et al. (2009) as being symptomatic of using
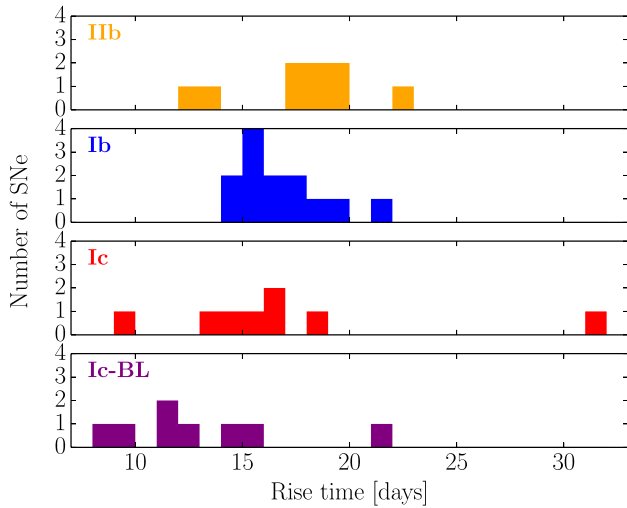
Figure 6. Rise times of SE SNe subtypes in the sample as estimated from the fitting of the analytical model. SNe IIb, Ib and Ic share similar average rise times (17.6, 16.7, 16.8 d, respectively), with SNe Ic-BL somewhat faster (13 d).

a single opacity and v_{ph} value in the model. In contrast, Tanaka et al. shows SN 2008D displayed strong evolution in v_{ph}, with BL early on, before becoming more normal SN Ibc-like around peak. Since the v_{ph} in the model is that at peak, the presence of this early, highly energetic evolution has no impact on the derived parameters. A lower value of κ_{opt} in the model would work to bring values in better agreement. The bolometric light curve of Tanaka et al. (2009) was constructed directly from UV-optical-NIR photometry. There is overall good agreement in the shape of the light curves but a ~0.1 mag increase in brightness of the light curve created using the BCs here – this is likely to be a contributing factor to the higher M_{Ni} value we find here. Additionally, we note our M_{ej} is significantly less than the ~7 $M_{\odot}$ derived by Mazzali et al. (2008) through spectral modelling.

SN 2011dh. For comparison, we use the parameters of Ergon et al. (2014), which revise those used in Bersten et al. (2012) where initial modelling of SN 2011dh was performed, in order to compare to their hydrodynamical modelling results. Bersten et al. (2012, updated in Ergon et al. 2014) find $M_{Ni} = 0.075$ $M_{\odot}$, $M_{ej} = 1.8$–2.5 $M_{\odot}$ and $E_K = 0.6$–1.0 $\times 10^{51}$ erg, where the modelling presented here gives $M_{Ni} = 0.08$ $M_{\odot}$, $M_{ej} = 2.2$ $M_{\odot}$ and $E_K = 0.7 \times 10^{51}$ erg. Estimates of each parameter are in good agreement. The bolometric light curve modelled by previous work is constructed directly from photometry of SN 2011dh from UV–MIR. Our reconstructed bolometric light curve is in very good agreement, which is not unexpected since SN 2011dh formed part of the sample used in the construction of the BCs.

SN 2011hs. The distance and reddening to SN 2011hs were set as in Bufano et al. (2014), however the authors note a large uncertainty on the time of explosion: $t_0 = 2455872 \pm 4$ JD. Bufano et al. (2014) find $M_{Ni} = 0.04$ $M_{\odot}$, $M_{ej} = 1.8$–2.5 $M_{\odot}$ and $E_K = 0.8$–0.9 $\times 10^{51}$ erg using the mid-point of the t_0 range. When fixing t_0 to 2455872 JD, we obtain values of $M_{Ni} \sim 0.05$ $M_{\odot}$, $M_{ej} = 2.3$ $M_{\odot}$ and $E_K = 0.9 \times 10^{51}$ erg. Although this gives values in very good agreement, it must be stressed the overall fit is poor. The model appears better fitted with a later t_0, which explains the difference between our estimates in Table 5 and those when fixing to t_0 here, furthermore, an earlier t_0 is favoured by radio observations (Bufano et al. 2014).

Given the extended nature of the progenitor star, the model here may not be as appropriate for such explosions. The bolometric light curve of SN 2011hs was created by Bufano et al. (2014) through direct integration of photometry covering a wide wavelength range (UV-optical-NIR), and we find good agreement to our light curve.

iPTF13bvn. The reddening and distance in Table 1 for iPTF13bvn are those of Fremling et al. (2014), and here t_0 is fixed to their adopted value of 2456459.25 JD. They obtain parameters of $M_{Ni} = 0.04$–0.07 $M_{\odot}$, $M_{ej} = 1.3$–2.4 $M_{\odot}$ and $E_K = 0.5$–1.4$\times 10^{51}$ erg. The results of the modelling presented here gives $M_{Ni} = 0.06$ $M_{\odot}$, $M_{ej} = 1.9$ $M_{\odot}$ and $E_K = 0.7\times 10^{51}$ erg. When adopting the values presented in Bersten et al. (2014), namely $E(B - V) = 0.21 \pm 0.03$ mag and $\mu = 32.04 \pm 0.2$ mag, the results are $M_{Ni} = 0.11$ $M_{\odot}$, $M_{ej} = 1.8$ $M_{\odot}$ and $E_K = 0.7\times 10^{51}$ erg compared to the values of Bersten et al. (2014): $M_{Ni} \sim 0.1$ $M_{\odot}$, $M_{ej} \sim 2.3$ $M_{\odot}$ and $E_K \sim 0.7 \times 10^{51}$ erg. The estimates from this simple modelling agree well with each of those found from hydrodynamical modelling by two groups. For Bersten et al. (2014), the bolometric light curve modelled was created using the BCs of LBJ14, as is done here, whereas Fremling et al. (2014) used optical photometry of iPTF13bvn alongside a UV and IR correction derived from SN 2011dh. There is good agreement between the bolometric light curves created through each method.

3.4 SN type distributions

With a sample of explosion parameters for many different SNe, the statistical distribution as a function of SN type can be investigated. The cumulative distributions of the parameters for each type are shown in Fig. 7. This figure highlights the extreme nature of SNe Ic-BL in M_{Ni} and E_K. SNe Ic-BL are more energetic than any of the other subtypes (the least energetic SN Ic-BL has an E_K value above the average value of any of the other subtypes), and also have much larger M_{Ni} values on average, although it should be noted that SNe Ib and Ic can reach such high M_{Ni} values even though the bulk have much lower values. However, M_{ej} distributions do not distinguish SNe Ic-BL from other SE SNe clearly. SNe Ib and Ic are indistinguishable in all three parameters. There appears to be a hint that SNe IIb favour lower values of M_{Ni} and E_K cf. SNe Ib and Ic, whereas their M_{ej} values do not show this. We note good agreement in the relative average explosion parameters between SN subtypes compared to Cano (2013), although numerical factor differences in the models compromise, good absolute agreement. Additionally, the large fraction of events for which an average v_{ph} (based on subtype) is assigned in Cano (2013) limits the usefulness of direct comparisons. However, both studies find similarity in the ejecta masses of SNe Ib, Ic and Ic-BL, similarity between SNe Ib and Ic in each parameter, and that SNe Ic-BL exhibit generally larger M_{Ni} and E_K values than other SN subtypes.

The two-sample Kolmogorov–Smirnov test (K–S test) was applied to each pair of SN types to ascertain the probability (p value) that the two samples are drawn from the same parent population given the maximum difference, D, between their cumulative distributions, where a small p value indicates that it is statistically unlikely the two samples are explained by a single population.[9] The results of the K–S test are given in Table 7, which confirm the 'by-eye' judgements on the distributions made above. The distribution of M_{Ni} values of (IIb, Ic-BL) are significantly different, with M_{Ni} values of (IIb, Ic), (Ib, Ic-BL) and (Ic, Ic-BL) distinguished

---

[9] Tests were repeated with the two-sample Anderson–Darling test, with significances remaining at very similar levels.
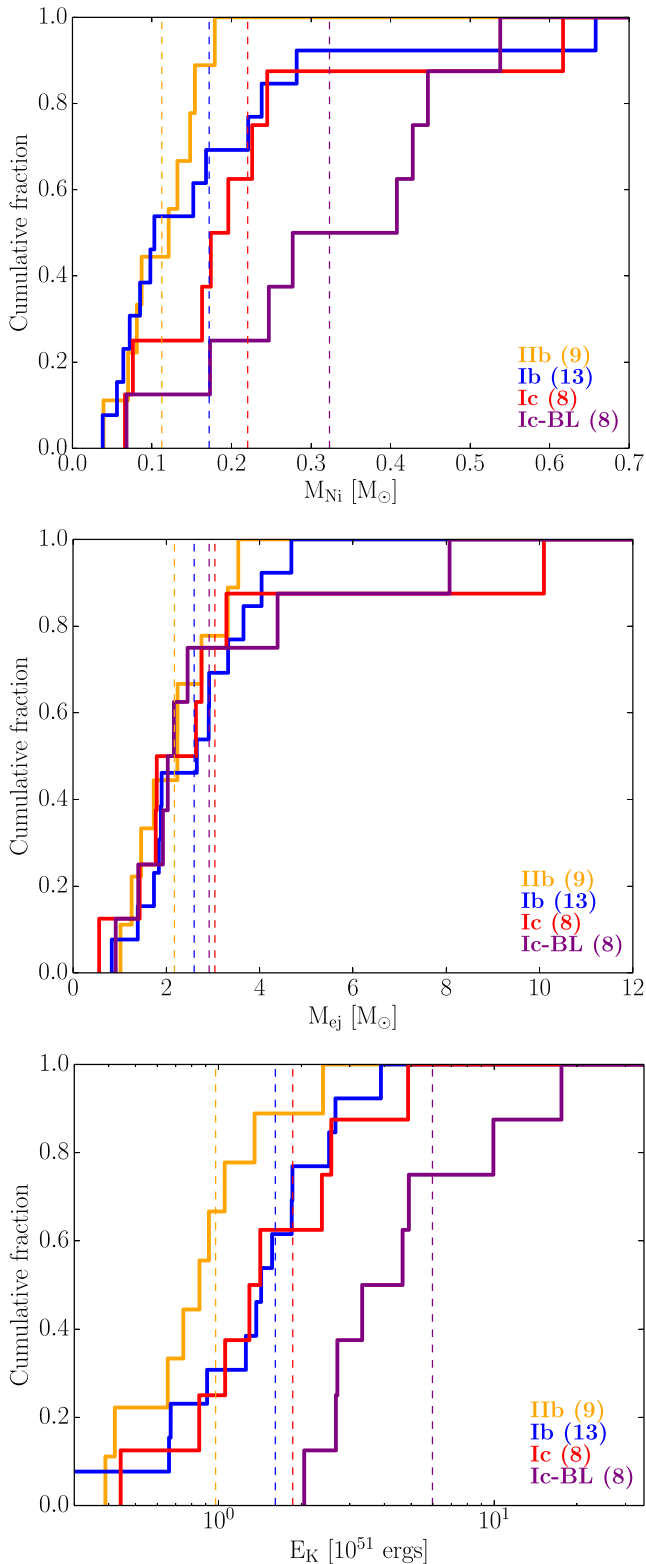
Figure 7. Cumulative distributions for explosion parameters of SE SNe (top: M_{Ni}, middle: M_{ej}, bottom: E_K, note logscale), divided by subtype. The average values for each SN type are indicated by the vertical dashed lines.

at a lower significance of $\sim 2\sigma$. The E_K distribution of SNe Ic-BL is statistically distinguished from those of SNe IIb, Ib and Ic. As expected, M_{ej} distributions cannot be distinguished and all four subtypes are consistent with being drawn from any of the other distributions. On the whole, SNe IIb, Ib and Ic are indistinguishable, although there is some marginal evidence of a difference in the M_{Ni} and E_K distributions of SNe IIb to those of SNe Ib and Ic.

An important caveat to consider when regarding comparison between the parameter distributions is that the sample was drawn from literature events. As such, many selection and observational biases are intrinsic to its creation. For example, it may be that we are skewing the M_{Ni} distribution for SNe Ic-BL by preferentially including bright SNe Ic-BL (i.e. high M_{Ni}) as SNe Ic-BL appear intrinsically rarer in the very local Universe than the other subtypes, whose distributions would therefore be less affected. Such caveats motivate a similar study on a more homogeneously created sample of SNe to further investigate the initial distribution comparisons of this study.

4 DISCUSSION

The results of this study provide for the first time a large sample of bolometric light curves of SE SNe, with which the nature of the explosions of various SNe types has been investigated.

4.1 Bolometric light curves

The bolometric light curves of SE SNe are diverse in M_{peak} and $\Delta m_{15,bol}$ within each subtype and as a whole. Plotting the decline rate and peak of each light curve indicates that early bolometric light curves alone cannot be used to reliably distinguish between SE SN types (Fig. 2). Properties such as colour evolution remain a more promising avenue for distinguishing SE SNe in the absence of spectral information (e.g. Poznanski et al. 2002; Gal-Yam et al. 2004; Bianco et al. 2014) – a scenario that will be probable for the vast majority of SNe discovered by future SN surveys. The apparent M_{peak}–$\Delta m_{15,bol}$ inverse correlation for SNe Ic-BL (excluding SNe 2002ap and 2005kz) in Fig. 2 is akin to the suggestion of a possible Phillips' relation (i.e. brighter SNe have wider light curves; Phillips 1993) for GRB-SNe that is discussed in Schulze et al. (2014). Any possible relation will merit study as the sample of such events grows (as well as investigating the reasons behind outliers, should a relation present itself). Three of the events that appear to sit along the supposed relation did not show evidence of an associated high-energy component (2003jd, Valenti et al. 2008; 2007ru, Sahu et al. 2009; 2009bb, Pignata et al. 2011, although strong radio emission suggests the presence of relativistic material in this SN; Soderberg et al. 2010). The standardizing of GRB-SN light curves has been further studied by Cano (2014) and Li & Hjorth (2014), who indeed find relations based on light-curve properties to allow their cosmological use, confirming the indications from the relatively cruder analyses in Schulze et al. (2014) and here.

4.2 Photospheric velocities

Although we use empirical measurements of v_{ph} for all but one of our sample (as opposed to relying on averages or fiducial values as has been done in similar previous studies) in order to reduce systematic biases, the data set used and methods employed are inherently heterogeneous.

In particular, one aspect to consider is the nature of the feature in SE SNe around 6200 Å. We attribute this to Si II λ6355 in order to determine v_{ph} for ~ 20 per cent of our sample, but this identification

Table 7. Results of two-sample KS test on explosion parameters between SE SN types.

Sample 1	Sample 2	M_{Ni}		M_{ej}		E_K	
		D	p	D	p	D	p
IIb	Ib	0.308	0.608	0.291	0.680	0.504	0.089
IIb	Ic	0.639	*0.034*	0.194	0.992	0.528	0.125
IIb	Ic-BL	0.764	**0.006**	0.250	0.915	0.889	**8×10^{-4}**
Ib	Ic	0.365	0.428	0.269	0.800	0.164	0.998
Ib	Ic-BL	0.596	*0.034*	0.289	0.727	0.798	**0.001**
Ic	Ic-BL	0.625	*0.050*	0.250	0.929	0.750	**0.010**

has been widely debated (e.g. Branch et al. 2002; Folatelli et al. 2006; Parrent et al. 2007; Tanaka et al. 2009; Hachinger et al. 2012; Parrent et al. 2015). These studies (and others) argue this feature may be explained as being due to unburnt hydrogen via the H α line, or some combination of H α and Si II λ6355. Other species have also been proposed as being responsible for this feature such as detached He I (Clocchiatti et al. 1996) or C II (Elmhamdi et al. 2006).

The nature of the absorption feature around 6200 Å is uncertain. We present some comparisons of velocities in the literature when it is attributed to Si II λ6355, compared to v_{ph} for the same SNe (determined from Fe II lines or via spectral modelling), in order to assess the impact of this potential misidentification. Gal-Yam et al. (2002) determine an Si II velocity (15 000 km s^{-1}) at peak for SN 2002ap that is in good agreement with the Fe II velocity determined here (13 000 km s^{-1}) considering the slight difference in epoch measured.[10] Folatelli et al. (2006) consider the absorption feature to be mainly or wholly due to H α for SN 2005bf since they find $v_{ph} \sim$ 7500 km s^{-1} around the first peak, whereas the velocity of Si II would be $\sim$4800 km s^{-1}. Tanaka et al. (2009) determine a v_{ph} for SN 2008D via spectral modelling of 9000 km s^{-1} and determine the velocity of Si II as 9300 km s^{-1} (Soderberg et al. 2008, also find a similar Si II velocity). Pignata et al. (2011) find their Fe II (λ4924, 5018, 5169) velocity to be 'a good match' to the one determined for Si II λ6355 for SN 2009bb near peak.

It should be noted that five out of eight of our v_{ph} measurements that rely on using an Si II λ6355 velocity are SNe Ic-BL (since the high velocities cause strong blending of the Fe II features). For the SNe Ic-BL 2002ap and 2009bb, where Fe II velocities could be measured, these are found to agree very well with those of Si II if the 6200 Å feature is so attributed. There appears to be the presence of a small amount of hydrogen in a mean SN Ib peak-light spectrum (see Liu & Modjaz 2015), which may mean the influence of H α on the 6200 Å feature is stronger for this subtype, however, we only use an Si II-determined velocity for one SN Ib. Although there clearly may be significant departures from the true v_{ph} when this feature is attributed to Si II λ6355, we only rely on this assignment for $\sim$20 per cent of events and a number of those are likely to produce consistent velocities to their v_{ph}. We thus do not consider this potential misidentification to significantly affect overall conclusions and results, although of course it is an additional source of uncertainty for these individual events.

In agreement with the new results of Liu & Modjaz (2015), based on their analysis of Fe II λ5169 in a large number of SE SNe spectra, and with consideration to the above caveats, we find an increasing average v_{ph} for the subtypes following SNe IIb → Ib → Ic although the significant spread in values within any one subtype means there

exists significant overlap between SNe IIb, Ib and Ic, with SNe Ic-BL (unsurprisingly, given the nature of their classification) at higher velocities.

4.3 Explosion parameters

The results of the simple modelling presented here agree for the majority of events where more detailed analysis has been performed to extract explosion parameters. Where results differ, it is generally the case that values are lower than other modelling. Differences for some SNe are likely to be due to the simplifications in the analytical model, which does not account for, e.g. velocity or opacity evolution, asymmetries in the explosion, or the presence of extended envelopes. Nevertheless, these results require just two-filter optical observations and a single spectrum of each SN (compared to multiband UV/optical/NIR photometry and at least several epochs of spectral coverage, required for more detailed modelling). The bolometric light-curve creation method used (LBJ14) also appears robust to all well-observed SE SNe thus far and hence no large uncertainties on the results are being introduced through its use (for example, the typical error in a host distance modulus is larger than the $\lesssim$0.1 mag rms on the BC fits). Even so, it is imperative that detailed modelling of SNe with much larger data sets continues apace. This is required not only for the intrinsic in-depth knowledge of SN explosions such studies afford, but also to act as a basis for assessing the consistency of coarser methods such as this for the future of data-starved SN studies, especially when including increasing samples of unusual events.

An interesting result is the similarity between SNe Ib and Ic in each of the parameters explored. The SNe are very similar in their bulk properties, i.e. the exploding cores of these SNe have similar masses and produce explosions with similar amounts of E_K and M_{Ni}. Exploding pre-SN stars producing SNe Ib must have a non-negligible mass of helium. However, the presence of helium in the progenitors of SNe Ic has been debated. The predictions of conflicting theoretical results, which argue for (Dessart et al. 2012; Piro & Morozova 2014) and against (Frey, Fryer & Young 2013) the presence of helium in SE SNe have been investigated by Liu & Modjaz (2015). These authors conclude that empirical differences in the spectra of SNe Ib and Ic are inconsistent with the predictions made by studies that suggest helium is hidden in SNe Ic, instead favouring very little to no helium being present. This is in agreement with results of radiative transfer models including non-local thermodynamical equilibrium effects of SE SNe (see Hachinger et al. 2012, and references therein), which suggest that only $\sim$0.1 M$_\odot$ is required in the progenitor star to produce an observable signature in the spectra. Assuming then SNe Ic lack any significant helium envelope mass, this would mean the carbon-oxygen (CO) core mass will be lower for an SN Ib with the same M_{ej} as a SN Ic. Since CO core mass increases with zero-age main sequence (ZAMS) mass of

---

[10] The Gal-Yam et al. (2002) Si II velocity is at B-band peak whereas ours is just after L_{bol} peak.

a progenitor, it follows that the ZAMS mass of an SN Ib would be expected to be lower than that of a Ic, for equal M_{ej}. The apparent similarity in the M_{ej} distributions shown here would then hint towards lower CO core masses (and thus lower ZAMS mass) for SNe Ib compared to Ic. However, as mentioned, the helium mass required to produce an SN Ib spectrum may be only ~ 0.1 M$_\odot$ (Hachinger et al. 2012). Considering this, alongside the comparatively large uncertainties on our M_{ej} values, the distributions cannot be used to rule conclusively on any potential mass sequence (or lack of) in the ZAMS masses of SNe Ib and Ic.

Despite the modest sample sizes (from a statistical viewpoint), the SNe Ic-BL manifest themselves as very different in two of the three explosion parameters determined here. Their M_{Ni} and E_K values are much larger on average than the distributions of any of the other SN types. However, unlike the E_K distributions, where even the least energetic SN Ic-BL is more energetic than the majority of SNe IIb, Ib and Ic, the largest M_{Ni} masses of SNe Ic-BL are matched by those of SNe Ib and Ic. This indicates the presence of BL is not a certainty when a large amount of M_{Ni} is synthesized (since we see SNe Ib and Ic with comparable M_{Ni}), and thus the peak brightness is not a uniquely determining factor. Additionally, although the high-velocity nature of SNe Ic-BL naturally implies a large E_K/M_{ej} ratio (equation 2), these large E_K/M_{ej} ratios are occurring at very similar M_{ej} values of the other SN subtypes (SNe Ic-BL are indistinguishable from the individual or combined IIb/Ib/Ic distribution), favouring an energy source that is decoupled from a dependence on the mass of the exploding core.

4.4 Explosion parameter correlations

The parameters derived from the modelling are plotted against each other in Fig. 8. The bulk of SNe IIb, Ib and Ic appear to form a fairly tight correlation in the M_{ej}–E_K plot, this is a result of the similar v_{ph} values they exhibit (which, in turn, gives the M_{ej}/E_K ratio). Conversely, SNe Ic-BL, which can have very high velocities (Table 4), are found at larger E_K/M_{ej} ratios, as dictated by equation (2). Some splitting of SNe Ic-BL occurs with the 'hypernova branch' (i.e. very high M_{ej} and E_K values; e.g. Mazzali et al. 2013) being populated by SNe 1998bw and 2005kz, whereas other SNe Ic-BL sit at similar M_{ej} values to other SN types, but with higher E_K values. SN 2011bm appears as an intermediate member of the hypernova branch in these plots, despite displaying very modest velocity, with $v_{ph} = 9000$ km s^{-1}. In this case, the huge explosion parameter values found were due to the extremely slow evolution of the SN (Valenti et al. 2012, Fig. 2), and could point to an alternative signature of the explosion of a very massive star, perhaps without the angular momentum to produce an accretion-disc powered jet. Although SN Ic-BL M_{ej} values have a similar distribution to those of other SE SN types, their M_{Ni} values (barring SN 2002ap) are much higher than the bulk of SE SNe, indicating the production of M_{Ni} is much more efficient in these explosions.

SNe IIb appear to be the most homogeneous subtype of SE SNe as evident from the clustering of their bolometric light-curve properties (Fig. 1) and explosion parameters (Fig. 8). This may be a result of a much more restrictive progenitor range for SNe IIb (e.g. Yoon et al. 2010).

Hamuy (2003) show a correlation of increasing E_K with M_{Ni} for SNe IIP and to a weaker extent this is also found for SE SNe. Although there is a large amount of scatter and SN 2005hg is a prominent outlier, a correlation between M_{Ni} and E_K can be seen in Fig. 8 – no highly energetic and M_{Ni} deficient events are seen. Similarly, a correlation between M_{Ni} and v_{50} (v_{ph} at 50 d after
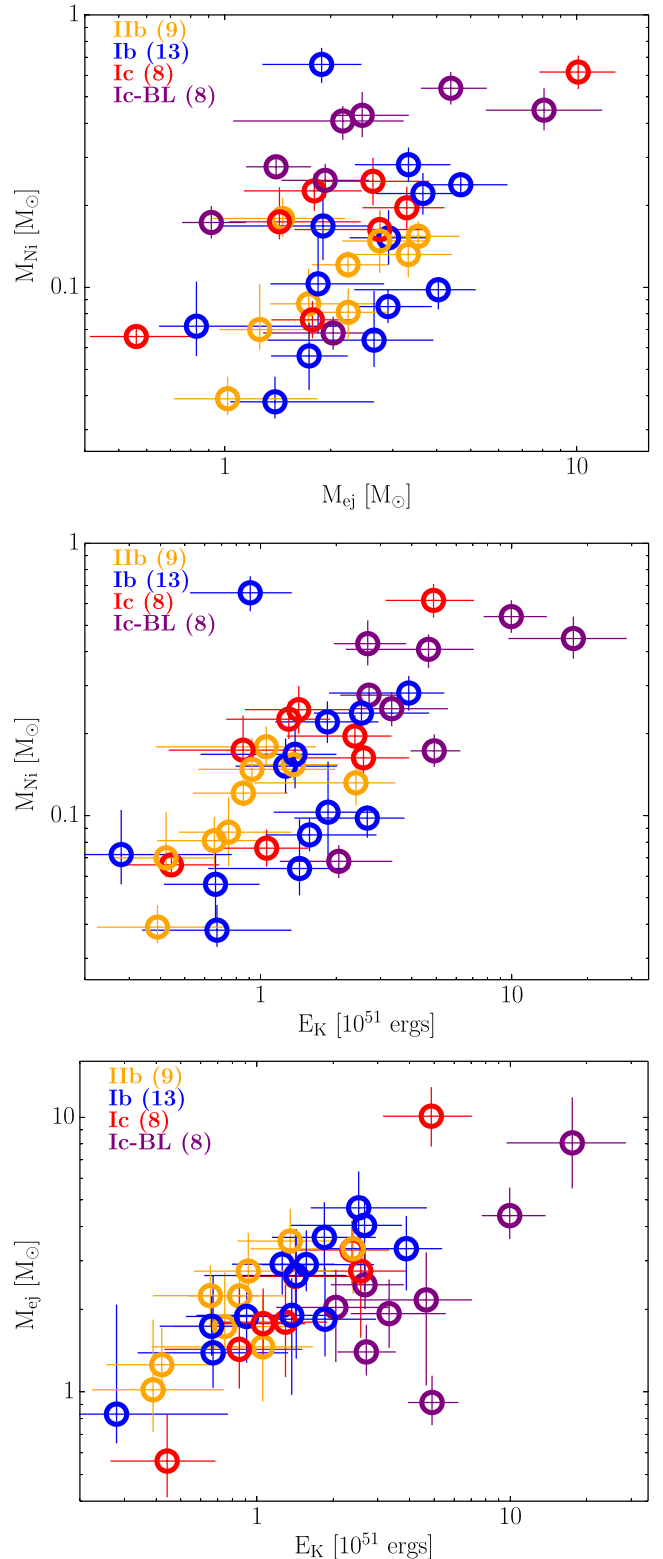

Figure 8. Derived explosion parameters (M_{Ni}, M_{ej} and E_K) of literature SE SNe are plotted against each other. Data are given in Table 5. SNe are colour-coded according to their type.
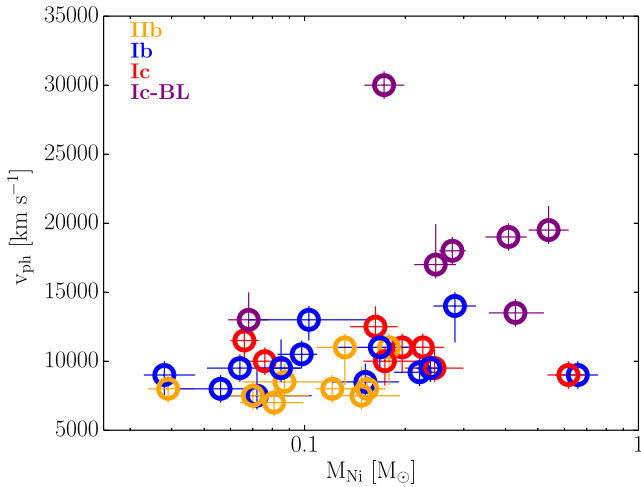
Figure 9. The M_{Ni} and v_{ph} values for SE SNe found from the modelling presented here. Only SNe with a directly measured v_{ph} are included. No clear indication of a single relation exists (cf. SNe IIP; see Hamuy 2003 and Spiro et al. 2014). SNe are colour-coded according to their type.

explosion) was shown for SNe IIP by Hamuy (2003), which was found to extend to underluminous SNe IIP by Spiro et al. (2014). Fig. 9 shows the analogous data for SE SNe, with the velocity here being defined as that at peak light (note that only SNe with a directly measured v_{ph} are included). There appears to be no strong dependence of M_{Ni} on v_{ph}, and indeed the average behaviour of the SNe IIb, Ib and Ic looks flat in v_{ph} over a wide range of M_{Ni} values.

4.5 The role of binaries as SE SNe progenitors

The question of whether massive single stars or binary systems are the progenitors of SE SNe is an area of active debate. The value of M_{ej} for an SN can be used to infer the nature of the progenitor system, by comparing to results from stellar evolution models. The M_{ej} values for each SN type were summed over the probability density functions of the M_{ej} values of individual SNe (assuming Gaussian errors) and normalized to give overall probability density functions for the SN types and entire sample. These functions are presented in Fig. 10, with M_{ej} values of 1–3 $M_\odot$ dominating. These low M_{ej} values are incompatible with the distributions of M_{ej} expected from massive, single WR stars ($Z = 0.008$ and 0.02). In Fig. 10, the observed distribution is compared to the stellar evolution models used in the binary population and spectral synthesis (BPASS) code (Eldridge et al. 2008; Eldridge & Stanway 2009).[11] The single star models in this set give no M_{ej} values lower than 5 $M_\odot$. The spread of M_{ej} values for stars of 20 $M_\odot < M_{init} \leq 150$ $M_\odot$ are shown in Fig. 10 – note although these seem low compared to some of the high M_{ej} SNe, these are conservative estimates, as discussed later, meaning the distribution is likely to extend to larger M_{ej} masses. Similarly, large M_{ej} values for single stars were found by Groh et al. (2013b), who show for an initial progenitor mass of $\sim$30 $M_\odot$, an SN Ib/c has $\simeq$7–8 $M_\odot$ of material beyond the remnant mass upon explosion. One must invoke more moderately massive progenitors in binary systems in order to reproduce the observed M_{ej} values. Binary models from the BPASS code with initial primary masses of 8–20 $M_\odot$ produce M_{ej} values that are in better agreement with the

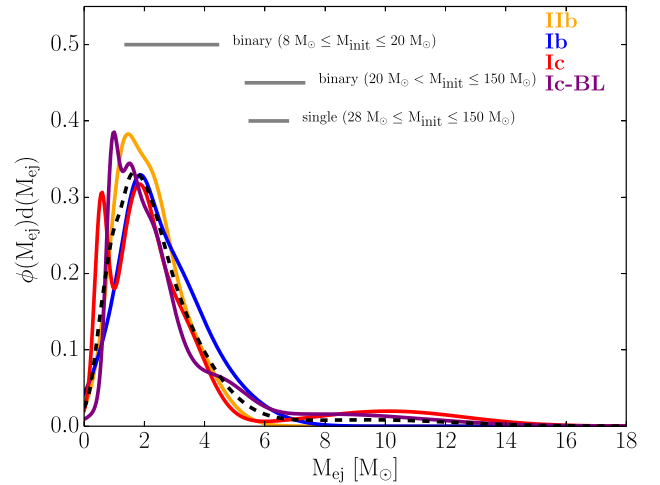[11] http://www.bpass.org.uk/

Figure 10. Probability density functions of SE SNe types for M_{ej}, found by summing the individual SNe in each type assuming Gaussian errors and normalizing the integrated area to one. The entire sample is shown by the black dashed line. Note the lower M_{ej} peak in the SN Ic distribution occurs solely due to SN 1994I. Also plotted are the one standard deviation ranges for the M_{ej} for binary and single stars from the BPASS models at $Z = 0.008$, values at solar metallicity are similar for $M_{init} \leq 20$ $M_\odot$ but larger on average for more massive stars. Note the values for M_{ej} of stars $M_{init} > 20$ $M_\odot$ are conservative, and are likely to extend to higher values (see the text, Fig. 11).

range of the observed distribution (Fig. 10). More massive progenitors evolving in binaries converge on similar M_{ej} values as single stars. Thus, although large M_{ej} events such as SN 2011bm cannot be distinguished as residing in a binary or not from this analysis, the probability density functions show that moderately massive (8 $M_\odot \leq M_{init} \leq 20$ $M_\odot$) binary progenitors are not only a necessary progenitor channel for each SE SNe type, but also that they dominate; only 5/38 of the sample are consistent with $M_{ej} > 5$ $M_\odot$. Such a result is in agreement with the findings of Eldridge et al. (2013). Furthermore, the selection effects associated with discovering and characterizing SNe should make these high-mass events favourable to observation (i.e. broad light curves) compared to the narrower, faster-declining SNe with lower mass progenitors. This gives confidence that a population of high-mass progenitor SNe are not being missed from the current SN survey strategies. Although we again stress that some M_{ej} values may be underestimated with this simple modelling scheme, even when considering only values in Table 5 from more detailed modelling, the same arguments hold; the majority of SNe having $M_{ej} \sim$ 1–3 $M_\odot$ and only 2/11 with $M_{ej} \gtrsim$ 5 $M_\odot$.

The model M_{ej} values for the more massive stars shown in Fig. 10 are conservative estimates. These were found using a canonical SN explosion energy of 10^{51} erg with a simple treatment of integrating the binding energy of the envelope inwards until it reached this explosion energy or to a point where the interior mass was 1.4 $M_\odot$, which we take as the minimum mass of the compact remnant. However, this energy is somewhat modest compared to most SN, in particular for larger M_{ej} SNe which exhibit $\gtrsim$3–10 $\times$ 10^{51} erg. The effect of increasing the unbinding energy by a factor 10 is shown in Fig. 11 for a range of binary models over all masses. This has little influence on the lower mass progenitors where the ejecta mass is roughly that of the final mass minus 1.4 $M_\odot$ for each energy used, and the spread of M_{ej} values from the models remains in good agreement with the observed peak around 2 $M_\odot$. For more massive
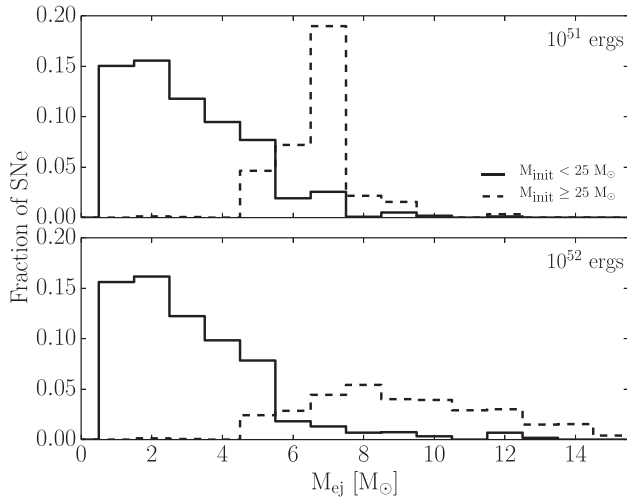
Figure 11. BPASS model predictions for the M_{ej} distribution of SE SNe weighted by the stellar IMF. The energy of the SN used was 10^{51} erg (top panel) and 10^{52} erg (bottom panel). Increasing the explosion energy has minimal effect on lower mass stars (solid lines), since even the lower energy case essentially unbinds all the outer core beyond a $1.4\,M_\odot$ compact remnant. For very massive stars (dashed lines), the additional energy allows more of the core to be ejected during the explosion, increasing the average M_{ej} and spread. This distribution is a good match to the high M_{ej} tail of the observed M_{ej} distribution (Fig. 10); however, it also contributes a much larger fraction of all SNe than is observed (see the text).

stars, the extra unbinding energy is able to liberate more of the outer core, reducing the size of the compact remnant (the effect is qualitatively the same for single massive stars). An unbinding energy of 10^{52} erg produces a spread of M_{ej} values that covers the observed very high M_{ej} events, and dilutes the strong peak at $M_{ej} \sim 7\,M_\odot$, which is not observed. In order to determine the fraction of SNe producing each bin of M_{ej}, the models were weighted by the IMF (Kroupa 2001). As can be seen, this treatment predicts that high M_{ej} events constitute a larger fraction of events than the observed distribution; for $M_{ej} > 5\,M_\odot$, the integrated observed probability density function is $\sim$10 per cent, whereas the 10^{52} erg models predict 35 per cent. Thus, although the spread of model M_{ej} values are good representations of the observed distribution, the quantitative divide between low- and high-M_{ej} events is inconsistent with expectations from the IMF, and something must act to suppress the observability of SNe from progenitors that would otherwise produce large M_{ej} explosions. Fall-back SNe, in which little or none of the mass is ejected or direct collapse to a black hole for very massive pre-SN progenitors could be possible solutions (e.g. Woosley 1993; Fryer 1999; Heger et al. 2003; Fryer et al. 2009; Kochanek 2014). This discrepancy will warrant further investigation with larger, more homogeneously selected observed samples and improved modelling.

One may expect very low M_{ej} systems to be more abundant, given some proportionality between the initial mass of the star and the exploding core mass, and considering the shape of the stellar IMF. For example, many more stars with final core masses of $\sim$2 $M_\odot$ (producing $M_{ej} \sim 0.6\,M_\odot$) are produced per galaxy than stars with final core masses $\sim$4–5 $M_\odot$ (producing $M_{ej} \sim 2.6$–$3.6\,M_\odot$). This is in contrast to our observations of a strong peak for SE SNe at $M_{ej} \sim$2–3 $M_\odot$ and a dearth of low M_{ej} values, $\lesssim 1\,M_\odot$ (Fig. 10), although it should be noted that we are observationally biased against such quickly evolving SNe, especially in regards to requiring

observations at, or prior to, peak. Low-mass He-stars, however, are formed from stars with ZAMS masses at the low end of the range for a CCSN. It is very difficult to remove the hydrogen envelope in such low-mass stars under normal circumstances (e.g. Yoon et al. 2010; Eldridge et al. 2013), and they will explode as hydrogen-rich SNe, and thus not form part of this sample by definition. Despite this, rapidly fading SNe such as, e.g. SN 2005ek (Drout et al. 2013, see also Drout et al. 2014) may represent very low M_{ej} systems, which observationally are SE SNe, indicating hydrogen-deficient explosions can occur within the lower mass range; modelling of 'ultrastripped' cores producing low M_{ej} SNe Ic as an explanation for these events has been performed by Tauris et al. (2013). However, considering binary evolution of the progenitors, a second binary mass transfer episode can occur in the later stages of stellar evolution. This mass transfer can occur during helium core or shell burning for low mass He-stars, which would otherwise ostensibly produce a CCSN (Habets 1986) – this can remove enough mass to prevent an explosion and instead result in a white dwarf (e.g. Delgado & Thomas 1981; Law & Ritter 1983; Dewi et al. 2002; Podsiadlowski et al. 2004). He-stars with $M \gtrsim 4\,M_\odot$ do not grow to a 'red giant' phase and do not undergo this mass transfer (Paczyński 1971; Delgado & Thomas 1981; Law & Ritter 1983). The more restrictive mass range in which a low-mass He-star can retain a core mass above the Chandrasekhar mass after undergoing mass transfer may provide additional theoretical support to explain the lack of low M_{ej} values, and the peak at $M_{ej} \sim 2$–$3\,M_\odot$ is then attributed to more massive He-stars, which do not undergo this mass transfer.

An outstanding issue is the use of a constant optical opacity, and its value, when performing analytical modelling for SE SNe. The values of M_{ej} are inversely proportional to the choice of κ_{opt}, and so we can ask what the value of κ_{opt} would need to be in order to shift the M_{ej} distribution to the point where it becomes consistent with the M_{ej} values of very massive stars ($\gtrsim$20–25 $M_\odot$). From Figs 10 and 11, a factor of 3 increase in the peak of the M_{ej} distribution would place it at the lower bound of very massive star ejecta masses. This corresponds to using $\kappa_{opt} = 0.02$ cm^2 g^{-1}. Although this is comparable to the suggested value for κ_{opt} from the study of Wheeler et al. (2015), this is outside the bounding range, $\sim$0.04–0.1 cm^2 g^{-1}, that is typically found via detailed modelling (e.g. Chugai 2000; Mazzali et al. 2000, 2013, Mazzali et al., in preparation). We again further reiterate the inconsistency of the distribution of M_{ej} with very massive star ejecta predictions (Fig. 11; Groh et al. 2013b) solely from results of other modelling (Table 5), where more careful prescriptions of the opacity are made.

4.6 The progenitors of SNe Ic-BL and GRB-SNe

SN Ic-BL and GRB-SN have been suggested to be more massive (younger) than their lower velocity counterparts (e.g. Larsson et al. 2007; Raskin et al. 2008; Svensson et al. 2010; Sanders et al. 2012; Cano 2013). Unfortunately, the sample of confirmed GRB-SN to which this method is applied is limited to three low-redshift events, SNe 1998bw, 2006aj and 2010bh, with the high-energy component of SN 2006aj being an X-ray flash. Notwithstanding having only three objects in the sample, when extracted from the SN Ic-BL sample, they are inconsistent with SNe IIb, Ib and Ic distributions in E_K (K–S test reveals $p \sim 1$–2 per cent), but cannot be distinguished in M_{ej} or M_{Ni}. They also cannot be distinguished from the remaining SN Ic-BL sample (five events). M_{ej} values of SNe Ic-BL/GRB-SNe and SNe IIb, Ib and Ic, are indistinguishable, indicating SNe Ic-BL/GRB-SNe have similar exploding core masses as other SN types, unless a large fraction of the core mass is not being ejected

due to fall-back on to a compact remnant in SNe Ic-BL/GRB-SNe. A complication of disentangling GRB-SNe is the prospect of off-axis jets, which would be missed; although radio detections can inform on the presence of strongly relativistic material (e.g. SN 2009bb; Soderberg et al. 2010) and potentially infer an off-axis jet, current detection limits, the prospect of other radio-emitting mechanisms, and the overlap between relativistic and non-relativistic SN radio light curves currently makes this very difficult (Bietenholz et al. 2014).

The extreme nature of GRB-SNe (and, to a lesser extent, SNe Ic-BL) means the E_K and M_{ej} estimates here may be underestimates as we make no account of the contribution from a denser, inner core of material that will reveal itself only in the late-time light curves, and which may have a significant contribution in SNe Ic-BL (Maeda et al. 2003). Indeed for SN 1998bw, for which we can compare results to more detailed modelling, we find a lower M_{ej} and E_K, although for SN 2002ap our estimates are in reasonable agreement.

Other studies of GRB-SNe that have extracted explosion parameters have found similarly remarkable SNe accompanying the high-energy burst.[12] For example, SN 2003lw/GRB031203 was found to be best described by an explosion with $M_{Ni} \sim 0.55$ M$_\odot$, $M_{ej} \sim$ 13 M$_\odot$ and $E_K \sim 60 \times 10^{51}$ erg (Mazzali et al. 2006b), and SN 2012bz/GRB120422A had $M_{Ni} \sim 0.4$–0.6 M$_\odot$, $M_{ej} \sim 6$–7 M$_\odot$ and $E_K \sim 35 \times 10^{51}$ erg (Melandri et al. 2012; Schulze et al. 2014). Both these events populate the hypernova subset of SNe Ic-BL. Inclusion of such spectacular GRB-SNe would only serve to further distinguish them from 'normal' SE SNe and may begin to distinguish them from the more modest SN Ic-BL (see Cano 2013). Walker et al. (2014) give explosion parameters for all SNe Ic-BL from the literature, including several that did not meet the selection criteria for this sample, as well as those found for a new object, PTF 10qts. Their collection of explosion parameters generally agrees with those presented here for overlapping events. The M_{ej} values display a similar distribution to that seen here for all SE SNe (Fig. 10), i.e. predominantly events with a few M$_\odot$ of ejecta, and a smaller fraction displaying much larger M_{ej} that is indicative of a higher ZAMS mass progenitor ($M_{init} \gtrsim 25$–30 M$_\odot$).

5 SUMMARY

A large sample of SE SN bolometric light curves has been made through the use of BCs presented in LBJ14. Peak bolometric absolute magnitudes range from -16.3 to -19.2 mag, with both luminosity extremes occupied by an SN Ib. $\Delta m_{15,bol}$ values range from 0.20 to 1.37 mag, with SNe Ic making up the extremes of this distribution. The possibility of a Phillips-type relation for GRB-SNe, suggested by Schulze et al. (2014) and independently confirmed by Cano (2014) and Li & Hjorth (2014), is evident here for the bolometric light curves of the majority of the SNe Ic-BL sample.

The bolometric light curves were modelled using an analytical prescription utilizing the velocity of the photosphere at peak light. When directly comparing to other detailed modelling, there is general agreement in most parameters, but there are notable exceptions. For the cases where there is disagreement, limitations and assumptions in this modelling are likely to be compromising a good agreement by not accounting for the true nature of the explosion (e.g. extended supergiant progenitors, or strongly evolving photospheric

velocities). Nevertheless, similar analysis on large numbers of SNe with relatively little follow-up can be used to further analyse populations of SE SNe. We again stress the importance of detailed study of observationally favourable SNe to further quantify potential uncertainties arising from such a simple treatment of the explosions. Of great importance is to further test how valid the assumptions in such analytical models are for larger numbers of SNe, particularly in relation to using a single value to characterize each of the photospheric velocity and the opacity.

The extreme nature of SNe Ic-BL was shown, with their M_{Ni} and E_K distributions being distinct from other SE SNe types. Conversely, the M_{ej} values for SNe Ic-BL are very similar to those of SNe IIb, Ib and Ic. When specifically comparing to SNe Ic in M_{ej} (i.e. where M_{ej} will be that of the CO core minus the mass locked in a compact remnant, although see discussion in Section 4.3), it appears the mass of the core does not play a major role in determining the presence of BL features (i.e. large v_{ph}), and this must be dictated by another property of the core (e.g. composition or angular momentum).

M_{ej} values from all SN subtypes peak around 2 M$_\odot$; this is inconsistent with massive single star models, which predict M_{ej} values >5 M$_\odot$. Conversely, the introduction of a *dominant* binary population of moderate mass progenitors (8 M$_\odot \leq M_{init} \leq 20$ M$_\odot$) for SE SNe explains the M_{ej} distributions extremely well. This is additional support to direct imaging studies that appear to favour lower mass binary progenitors (e.g. SNe 1993J, 2011dh and iPTF 13bvn). The lack of very low M_{ej} values also agrees with He-star binary evolution modelling, in which these low-mass systems instead become a white dwarf due to mass transfer, or retain a hydrogen envelope and as such would not explode as SE SNe. The lack of large M_{ej} events is somewhat at odds from predictions of stellar models with a simple weighting from the IMF. Fall-back SNe or direct collapse to a black hole for very massive stars may alleviate this discrepancy by reducing the observability of the SNe of such stars. We additionally note that these arguments are also valid when considering only those M_{ej} values derived from more detailed modelling (see Table 5), in that ~ 2 out of 11 SNe have large M_{ej} determinations ($\gtrsim 5$ M$_\odot$) with the rest around 1–3 M$_\odot$.

The current small sample of GRB-SNe analysed here cannot be distinguished from SNe Ic-BL. SNe IIb, Ib and Ic are all similar in each of the explosion parameters analysed, with some indication that SNe IIb, the most homogeneous subtype in bolometric properties, are M_{Ni} deficient and have lower E_K values compared to SNe Ib and Ic. The average M_{Ni} and E_K values follow the same sequence of increasing value of IIb $\rightarrow$ Ib $\rightarrow$ Ic $\rightarrow$ Ic-BL, however the average M_{ej} values are very similar amongst the subtypes.

---

[12] Although there are two examples (GRBs 060505 and 060614) for which deep limits preclude all but extremely faint accompanying supernovae (e.g. Della Valle et al. 2006; Fynbo et al. 2006).

REFERENCES

Anderson J. P., James P. A., 2008, MNRAS, 390, 1527

Anderson J. P., Covarrubias R. A., James P. A., Hamuy M., Habergham S. M., 2010, MNRAS, 407, 2660

Anderson J. P., Habergham S. M., James P. A., Hamuy M., 2012, MNRAS, 424, 1372

Arcavi I. et al., 2010, ApJ, 721, 777

Arcavi I. et al., 2012, ApJ, 756, L30

Arnett W. D., 1982, ApJ, 253, 785

Barbon R., Benetti S., Cappellaro E., Patat F., Turatto M., Iijima T., 1995, A&AS, 110, 513

Benetti S. et al., 2011, MNRAS, 411, 2726

Benvenuto O. G., Bersten M. C., Nomoto K., 2013, ApJ, 762, 74

Bersten M. C., Benvenuto O., Hamuy M., 2011, ApJ, 729, 61

Bersten M. C. et al., 2012, ApJ, 757, 31

Bersten M. C. et al., 2014, AJ, 148, 68

Bianco F. B. et al., 2014, ApJS, 213, 19

Bietenholz M. F., De Colle F., Granot J., Bartel N., Soderberg A. M., 2014, MNRAS, 440, 821

Blinnikov S. I., Eastman R., Bartunov O. S., Popolitov V. A., Woosley S. E., 1998, ApJ, 496, 454

Blondin S., Modjaz M., Kirshner R., Challis P., Calkins M., 2006, Cent. Bur. Electron. Telegrams, 626, 1

Boissier S., Prantzos N., 2009, A&A, 503, 137

Branch D. et al., 2002, ApJ, 566, 1005

Bufano F. et al., 2014, MNRAS, 439, 1807

Cano Z., 2013, MNRAS, 434, 1098

Cano Z., 2014, ApJ, 794, 121

Cano Z. et al., 2011, ApJ, 740, 41

Cao Y. et al., 2013, ApJ, 775, L7

Chornock R. et al., 2010, preprint (arXiv:1004.2262)

Chugai N. N., 2000, Astron. Lett., 26, 797

Claeys J. S. W., de Mink S. E., Pols O. R., Eldridge J. J., Baes M., 2011, A&A, 528, A131

Clocchiatti A., Wheeler J. C., Brotherton M. S., Cochran A. L., Wills D., Barker E. S., Turatto M., 1996, ApJ, 462, 462

Clocchiatti A., Suntzeff N. B., Covarrubias R., Candia P., 2011, AJ, 141, 163

Corsi A. et al., 2011, ApJ, 741, 76

Crockett R. M. et al., 2007, MNRAS, 381, 835

Crowther P. A., 2013, MNRAS, 428, 1927

Delgado A. J., Thomas H.-C., 1981, A&A, 96, 142

Della Valle M. et al., 2006, Nature, 444, 1050

Dessart L., Hillier D. J., Li C., Woosley S., 2012, MNRAS, 424, 2139

Dewi J. D. M., Pols O. R., Savonije G. J., van den Heuvel E. P. J., 2002, MNRAS, 331, 1027

Drout M. R. et al., 2011, ApJ, 741, 97

Drout M. R. et al., 2013, ApJ, 774, 58

Drout M. R. et al., 2014, ApJ, 794, 23

Eldridge J. J., Stanway E. R., 2009, MNRAS, 400, 1019

Eldridge J. J., Izzard R. G., Tout C. A., 2008, MNRAS, 384, 1109

Eldridge J. J., Fraser M., Smartt S. J., Maund J. R., Crockett R. M., 2013, MNRAS, 436, 774

Eldridge J. J., Fraser M., Maund J. R., Smartt S. J., 2015, MNRAS, 446, 2689

Elmhamdi A., Danziger I. J., Branch D., Leibundgut B., Baron E., Kirshner R. P., 2006, A&A, 450, 305

Ergon M. et al., 2014, A&A, 562, A17

Filippenko A. V., 1997, ARA&A, 35, 309

Filippenko A. V., Foley R. J., Matheson T., 2005, IAU Circ., 8639, 2

Folatelli G. et al., 2006, ApJ, 641, 1039

Folatelli G. et al., 2014a, ApJ, 792, 7

Folatelli G. et al., 2014b, ApJ, 793, L22

Foley R. J. et al., 2003, PASP, 115, 1220

Fox O. D. et al., 2014, ApJ, 790, 17

Fraser M. et al., 2011, MNRAS, 417, 1417

Fraser M. et al., 2012, ApJ, 759, L13

Fremling C. et al., 2014, A&A, 565, 114

Frey L. H., Fryer C. L., Young P. A., 2013, ApJ, 773, L7

Fryer C. L., 1999, ApJ, 522, 413

Fryer C. L. et al., 2009, ApJ, 707, 193

Fynbo J. P. U. et al., 2006, Nature, 444, 1047

Gal-Yam A., Leonard D. C., 2009, Nature, 458, 865

Gal-Yam A., Ofek E. O., Shemmer O., 2002, MNRAS, 332, L73

Gal-Yam A., Poznanski D., Maoz D., Filippenko A. V., Foley R. J., 2004, PASP, 116, 597

Galama T. J. et al., 1998, Nature, 395, 670

Groh J. H., Georgy C., Ekström S., 2013a, A&A, 558, L1

Groh J. H., Meynet G., Georgy C., Ekström S., 2013b, A&A, 558, A131

Habets G. M. H. J., 1986, A&A, 167, 61

Hachinger S., Mazzali P. A., Taubenberger S., Hillebrandt W., Nomoto K., Sauer D. N., 2012, MNRAS, 422, 70

Hammer N. J., Janka H.-T., Müller E., 2010, ApJ, 714, 1371

Hamuy M., 2003, ApJ, 582, 905

Hamuy M. et al., 2002, AJ, 124, 417

Hamuy M. et al., 2009, ApJ, 703, 1612

Harutyunyan A. H. et al., 2008, A&A, 488, 383

Hasubick W., Hornoch K., 2002, IAU Circ., 7820, 4

Heger A., Fryer C. L., Woosley S. E., Langer N., Hartmann D. H., 2003, ApJ, 591, 288

Hjorth J., Bloom J. S., 2012, in Kouveliotou C., Wijers R. A. M. J., Woosley S., eds, The Gamma-Ray Burst - Supernova Connection. Cambridge Univ. Press, Cambridge, p. 169

Hunter D. J. et al., 2009, A&A, 508, 371

Iwamoto K., Nomoto K., Hoflich P., Yamaoka H., Kumagai S., Shigeyama T., 1994, ApJ, 437, L115

Iwamoto K. et al., 1998, Nature, 395, 672

Iwamoto K. et al., 2000, ApJ, 534, 660

Jerkstrand A., Fransson C., Kozma C., 2011, A&A, 530, A45

Jerkstrand A., Ergon M., Smartt S. J., Fransson C., Sollerman J., Taubenberger S., Bersten M., Spyromilio J., 2015, A&A, 573, 12

Kasliwal M. M. et al., 2010, ApJ, 723, L98

Kelly P. L., Kirshner R. P., 2012, ApJ, 759, 107

Kelly P. L., Filippenko A. V., Modjaz M., Kocevski D., 2014, ApJ, 789, 23

Kobulnicky H. A., Fryer C. L., 2007, ApJ, 670, 747

Kochanek C. S., 2014, ApJ, 785, 28

Kochanek C. S., Khan R., Dai X., 2012, ApJ, 759, 20

Kroupa P., 2001, MNRAS, 322, 231

Kuncarayakti H. et al., 2013, AJ, 146, 30

Larsson J., Levan A. J., Davies M. B., Fruchter A. S., 2007, MNRAS, 376, 1285

Law W. Y., Ritter H., 1983, A&A, 123, 33

Leloudas G. et al., 2011, A&A, 530, A95

Li X., Hjorth J., 2014, preprint (arXiv:1407.3506)

Li W., Wang X., Van Dyk S. D., Cuillandre J.-C., Foley R. J., Filippenko A. V., 2007, ApJ, 661, 1013

Li W., Chornock R., Leaman J., Filippenko A. V., Poznanski D., Wang X., Ganeshalingam M., Mannucci F., 2011, MNRAS, 412, 1473

Liu Y.-Q., Modjaz M., 2015, preprint (arXiv:1405.1437)

Lyman J. D., Bersier D., James P. A., 2014, MNRAS, 437, 3848 (LBJ14)

Maeda K., Mazzali P. A., Deng J., Nomoto K., Yoshii Y., Tomita H., Kobayashi Y., 2003, ApJ, 593, 931

Maeda K. et al., 2007, ApJ, 666, 1069

Maeda K. et al., 2008, Science, 319, 1220

Matheson T., Filippenko A. V., Ho L. C., Barth A. J., Leonard D. C., 2000, AJ, 120, 1499

Matthews K., Neugebauer G., Armus L., Soifer B. T., 2002, AJ, 123, 753

Mattila S., Meikle P., Chambers K., 2002, IAU Circ., 7820, 1

Maund J. R., Smartt S. J., 2005, MNRAS, 360, 288

Maund J. R., Smartt S. J., Kudritzki R. P., Podsiadlowski P., Gilmore G. F., 2004, Nature, 427, 129

Maund J. R., Wheeler J. C., Patat F., Baade D., Wang L., Höflich P., 2007a, A&A, 475, L1

Maund J. R., Wheeler J. C., Patat F., Wang L., Baade D., Höflich P. A., 2007b, ApJ, 671, 1944

Maund J. R. et al., 2011, ApJ, 739, L37

Maurer I., Mazzali P. A., Taubenberger S., Hachinger S., 2010, MNRAS, 409, 1441

Mazzali P. A., Lucy L. B., 1993, A&A, 279, 447

Mazzali P. A., Iwamoto K., Nomoto K., 2000, ApJ, 545, 407

Mazzali P. A., Nomoto K., Cappellaro E., Nakamura T., Umeda H., Iwamoto K., 2001, ApJ, 547, 988

Mazzali P. A. et al., 2005, Science, 308, 1284

Mazzali P. A. et al., 2006a, Nature, 442, 1018

Mazzali P. A. et al., 2006b, ApJ, 645, 1323

Mazzali P. A. et al., 2007, ApJ, 670, 592

Mazzali P. A. et al., 2008, Science, 321, 1185

Mazzali P. A., Deng J., Hamuy M., Nomoto K., 2009, ApJ, 703, 1624

Mazzali P. A., Walker E. S., Pian E., Tanaka M., Corsi A., Hattori T., Gal-Yam A., 2013, MNRAS, 432, 2463

Melandri A. et al., 2012, A&A, 547, A82

Mirabal N., Halpern J. P., An D., Thorstensen J. R., Terndrup D. M., 2006, ApJ, 643, L99

Modjaz M., 2007, PhD thesis, Harvard University

Modjaz M., Kirshner R., Challis P., Matheson T., 2005a, Cent. Bur. Electron. Telegrams, 267, 1

Modjaz M., Kirshner R., Challis P., Matheson T., Berlind P., 2005b, Cent. Bur. Electron. Telegrams, 271, 1

Modjaz M. et al., 2009, ApJ, 702, 226

Modjaz M., Kewley L., Bloom J. S., Filippenko A. V., Perley D., Silverman J. M., 2011, ApJ, 731, L4

Modjaz M. et al., 2014, AJ, 147, 99

Motohara K., Nomoto K., Gerardy C., Fesen R., Henry P., 2002, IAU Circ., 7834, 2

Nakamura T., Mazzali P. A., Nomoto K., Iwamoto K., 2001, ApJ, 550, 991

Ohta K., Maemura H., Ishigaki T., Aoki K., Ohtani H., 1994, PASJ, 46, 117

Olivares E. F. et al., 2012, A&A, 539, A76

Paczyński B., 1971, Acta Astron., 21, 1

Parrent J. et al., 2007, PASP, 119, 135

Parrent J. T., Milisavljevic D., Soderberg A. M., Parthasarathy M., 2015, preprint (arXiv:1505.06645)

Pastorello A. et al., 2008, MNRAS, 389, 955

Patat F. et al., 2001, ApJ, 555, 900

Perets H. B. et al., 2010, Nature, 465, 322

Phillips M. M., 1993, ApJ, 413, L105

Pian E. et al., 2006, Nature, 442, 1011

Pignata G. et al., 2011, ApJ, 728, 14

Piro A. L., Morozova V. S., 2014, ApJ, 792, L11

Podsiadlowski P., Joss P. C., Hsu J. J. L., 1992, ApJ, 391, 246

Podsiadlowski P., Hsu J. J. L., Joss P. C., Ross R. R., 1993, Nature, 364, 509

Podsiadlowski P., Langer N., Poelarends A. J. T., Rappaport S., Heger A., Pfahl E., 2004, ApJ, 612, 1044

Pols O. R., Dewi J. D. M., 2002, PASA, 19, 233

Poznanski D., Gal-Yam A., Maoz D., Filippenko A. V., Leonard D. C., Matheson T., 2002, PASP, 114, 833

Prieto J. L., Stanek K. Z., Beacom J. F., 2008, ApJ, 673, 999

Qiu Y., Li W., Qiao Q., Hu J., 1999, AJ, 117, 736

Raskin C., Scannapieco E., Rhoads J., Della Valle M., 2008, ApJ, 689, 358

Richmond M. W., Treffers R. R., Filippenko A. V., Paik Y., Leibundgut B., Schulman E., Cox C. V., 1994, AJ, 107, 1022

Richmond M. W. et al., 1996, AJ, 111, 327

Riffeser A., Goessl C. A., Ries C., 2002, IAU Circ., 7825, 2

Roy R. et al., 2013, MNRAS, 434, 2032

Ryder S. D., Murrowood C. E., Stathakis R. A., 2006, MNRAS, 369, L32

Sahu D. K., Tanaka M., Anupama G. C., Gurugubelli U. K., Nomoto K., 2009, ApJ, 697, 676

Sana H., Evans C. J., 2011, in Wade G., Meynet G., Peters G., eds, Proc. IAU Symp. 474, Active OB Stars: Structure, Evolution, Mass-Loss, and Critical Limits. Cambridge Univ. Press, Cambridge, p. 210

Sana H. et al., 2012, Science, 337, 444

Sanders N. E. et al., 2012, ApJ, 758, 132

Sauer D. N., Mazzali P. A., Deng J., Valenti S., Nomoto K., Filippenko A. V., 2006, MNRAS, 369, 1939

Schulze S. et al., 2014, A&A, 566, 102

Shivvers I. et al., 2013, MNRAS, 436, 3614

Smartt S. J., 2009, ARA&A, 47, 63

Smartt S. J., Maund J. R., Hendry M. A., Tout C. A., Gilmore G. F., Mattila S., Benn C. R., 2004, Science, 303, 499

Smith N., 2014, ARA&A, 52, 487

Smith N., Li W., Filippenko A. V., Chornock R., 2011, MNRAS, 412, 1522

Soderberg A. M. et al., 2008, Nature, 453, 469

Soderberg A. M. et al., 2010, Nature, 463, 513

Spiro S. et al., 2014, MNRAS, 439, 2873

Stanek K. Z. et al., 2003, ApJ, 591, L17

Stritzinger M. et al., 2002, AJ, 124, 2100

Stritzinger M. et al., 2009, ApJ, 696, 713

Svensson K. M., Levan A. J., Tanvir N. R., Fruchter A. S., Strolger L.-G., 2010, MNRAS, 405, 57

Taddia F. et al., 2015, A&A, 574, 60

Takada-Hidai M., Aoki W., Zhao G., 2002, PASJ, 54, 899

Tanaka M. et al., 2009, ApJ, 692, 1131

Taubenberger S. et al., 2006, MNRAS, 371, 1459

Taubenberger S. et al., 2011, MNRAS, 413, 2140

Tauris T. M., Langer N., Moriya T. J., Podsiadlowski P., Yoon S.-C., Blinnikov S. I., 2013, ApJ, 778, L23

Tominaga N. et al., 2005, ApJ, 633, L97

Tsvetkov D. Y., Volkov I. M., Baklanov P., Blinnikov S., Tuchin O., 2009, Perem. Zvezdy, 29, 2

Utrobin V., 1994, A&A, 281, L89

Utrobin V. P., Chugai N. N., 2008, A&A, 491, 507

Utrobin V. P., Chugai N. N., 2009, A&A, 506, 829

Valenti S. et al., 2008, MNRAS, 383, 1485

Valenti S. et al., 2011, MNRAS, 416, 3138

Valenti S. et al., 2012, ApJ, 749, L28

Van Dyk S. D., Li W., Filippenko A. V., 2003, PASP, 115, 1289

Van Dyk S. D. et al., 2012, AJ, 143, 19

Van Dyk S. D. et al., 2013, ApJ, 772, 32

Walker E. S. et al., 2014, MNRAS, 442, 2768

Walmswell J. J., Eldridge J. J., 2012, MNRAS, 419, 2054

Wang L., Wheeler J. C., 2008, ARA&A, 46, 433

Wang L., Howell D. A., Höflich P., Wheeler J. C., 2001, ApJ, 550, 1030

Wang L., Baade D., Höflich P., Wheeler J. C., 2003, ApJ, 592, 457

Wheeler J. C., Johnson V., Clocchiatti A., 2015, MNRAS, 450, 1295

Williams B. F., Peterson S., Murphy J., Gilbert K., Dalcanton J. J., Dolphin A. E., Jennings Z. G., 2014, ApJ, 791, 105

Woosley S. E., 1993, ApJ, 405, 273

Woosley S. E., Eastman R. G., Weaver T. A., Pinto P. A., 1994, ApJ, 429, 300

Yaron O., Gal-Yam A., 2012, PASP, 124, 668

Yoon S.-C., Woosley S. E., Langer N., 2010, ApJ, 725, 940

Yoon S.-C., Gräfener G., Vink J. S., Kozyreva A., Izzard R. G., 2012, A&A, 544, L11

Yoshii Y. et al., 2003, ApJ, 592, 467

Young T. R., Baron E., Branch D., 1995, ApJ, 449, L51

APPENDIX A: TEMPLATE BOLOMETRIC LIGHT CURVES

Table A1 shows the data for the template bolometric light curves of the various SN types shown in Fig. 3. The phases are with respect to the peak of L_{bol} and the median luminosity and standard deviation are given (as determined from the spread of luminosities of SNe that have data at that phase).

Table A1. Template bolometric light-curve data for SE SNe.

Phase (d)	IIb $\log_{10}L_{\rm bol}$ (erg s^{-1})	Std. dev.	Ib $\log_{10}L_{\rm bol}$ (erg s^{-1})	Std. dev.	Ic $\log_{10}L_{\rm bol}$ (erg s^{-1})	Std. dev.	Ic-BL $\log_{10}L_{\rm bol}$ (erg s^{-1})	Std. dev.
−18	42.155	0.560	41.582	0.317	–	–	–	–
−17	42.113	0.452	41.810	0.264	–	–	–	–
−16	42.073	0.339	41.865	0.214	–	–	–	–
−15	41.899	0.281	41.924	0.177	–	–	–	–
−14	41.888	0.260	41.996	0.159	–	–	–	–
−13	41.965	0.211	41.965	0.340	–	–	–	–
−12	41.956	0.166	42.042	0.332	–	–	–	–
−11	42.038	0.144	42.108	0.324	–	–	–	–
−10	42.119	0.130	42.163	0.313	–	–	–	–
−9	42.157	0.202	42.209	0.302	–	–	–	–
−8	42.178	0.198	42.397	0.387	42.506	0.185	–	–
−7	42.233	0.183	42.309	0.356	42.498	0.264	–	–
−6	42.276	0.172	42.394	0.352	42.634	0.231	–	–
−5	42.314	0.166	42.417	0.352	42.580	0.258	42.883	0.281
−4	42.342	0.162	42.397	0.339	42.601	0.236	42.923	0.254
−3	42.428	0.184	42.450	0.328	42.581	0.205	42.926	0.254
−2	42.440	0.182	42.460	0.329	42.595	0.197	42.923	0.254
−1	42.447	0.181	42.467	0.329	42.603	0.193	42.915	0.254
0	42.450	0.181	42.469	0.329	42.641	0.181	42.903	0.254
1	42.448	0.181	42.467	0.329	42.634	0.182	42.887	0.255
2	42.442	0.181	42.460	0.329	42.625	0.184	42.869	0.254
3	42.433	0.182	42.448	0.329	42.615	0.189	42.849	0.254
4	42.404	0.183	42.432	0.329	42.603	0.194	42.828	0.254
5	42.370	0.184	42.413	0.330	42.590	0.201	42.806	0.254
6	42.333	0.186	42.390	0.330	42.577	0.209	42.784	0.253
7	42.295	0.188	42.365	0.331	42.561	0.217	42.763	0.253
8	42.256	0.190	42.338	0.331	42.545	0.226	42.741	0.252
9	42.219	0.192	42.312	0.332	42.528	0.235	42.714	0.252
10	42.185	0.194	42.286	0.332	42.510	0.244	42.689	0.251
11	42.155	0.196	42.261	0.333	42.491	0.253	42.665	0.251
12	42.129	0.197	42.238	0.333	42.472	0.262	42.642	0.251
13	42.106	0.198	42.215	0.332	42.446	0.271	42.621	0.252
14	42.088	0.199	42.192	0.332	42.418	0.279	42.600	0.253
15	42.073	0.199	42.169	0.331	42.390	0.287	42.605	0.272
16	42.060	0.199	42.144	0.330	42.363	0.294	42.579	0.275
17	42.049	0.199	42.126	0.340	42.338	0.301	42.554	0.279
18	42.038	0.200	42.103	0.339	42.313	0.307	42.530	0.283
19	42.026	0.200	42.139	0.337	42.290	0.313	42.508	0.288
20	42.014	0.201	42.117	0.336	42.269	0.318	42.486	0.293
21	42.001	0.202	42.096	0.333	42.249	0.323	42.465	0.297
22	41.986	0.203	42.132	0.348	42.230	0.327	42.445	0.299
23	41.948	0.182	42.112	0.346	42.211	0.331	42.464	0.293
24	41.935	0.183	42.093	0.344	42.194	0.334	42.443	0.297
25	41.922	0.185	42.075	0.342	42.177	0.338	42.456	0.166
26	41.911	0.188	42.058	0.340	42.161	0.340	42.434	0.170
27	41.901	0.190	42.042	0.338	42.145	0.343	42.413	0.173
28	41.892	0.193	42.027	0.336	42.128	0.345	42.393	0.176
29	41.885	0.196	42.013	0.334	42.112	0.347	42.373	0.179
30	41.878	0.199	41.999	0.333	42.096	0.349	42.335	0.140

This paper has been typeset from a TEX/LATEX file prepared by the author.